This is an open access article published under an ACS AuthorChoice License, which permits copying and redistribution of the article or any adaptations for non-commercial purposes.

ACS OMEGA

Article

http://pubs.acs.org/journal/acsodf

Naphthalenediimide-Linked Bisbenzimidazole Derivatives as Telomeric G-Quadruplex-Stabilizing Ligands with Improved Anticancer Activity

Souvik Sur,[†,⊥] Vinod Tiwari,[†,⊥] Devapriya Sinha,[†,⊥] Mohammad Zahid Kamran,[‡] Kshatresh Dutta Dubey,[§] Gopinatha Suresh Kumar,[∥] and Vibha Tandon*[,†,‡]

[†]Chemical Biology Laboratory, Department of Chemistry, University of Delhi, Delhi 110007, India

[‡]Special Center for Molecular Medicine, Jawaharlal Nehru University, New Delhi 110067, India

[§]Institute of Chemistry, Hebrew University of Jerusalem, Jerusalem 91904, Israel

[∥]Biophysical Chemistry Laboratory, Chemistry Division, CSIR-Indian Institute of Chemical Biology, Kolkata 700032, India

Supporting Information

ABSTRACT: Human telomeric G-quadruplex DNA stabilization has emerged as an exciting novel approach for anticancer drug development. In the present study, we have designed and synthesized three C_2-symmetric bisubstituted bisbenzimidazole naphthalenediimide (NDI) ligands, **ALI-C$_3$**, **BBZ-ARO**, and **BBZ-AROCH$_2$**, which stabilize human telomeric G-quadruplex DNA with high affinity. Herein, we have studied the binding affinities and thermodynamic contributions of each of these molecules with G-quadruplex DNA and compared the same to those of the parent NDI analogue, **BMSG-SH-3**. Results of fluorescence resonance energy transfer and surface plasmon resonance demonstrate that these ligands have a higher affinity for G_4-DNA over duplex DNA and induce the formation of a G-quadruplex. The binding equilibrium constants obtained from the microcalorimetry studies of **BBZ-ARO**, **ALI-C$_3$**, and **BBZ-AROCH$_2$** were 8.47, 6.35, and 3.41 μM, respectively, with *h-telo* 22-mer quadruplex. These showed 10 and 100 times lower binding affinity with *h-telo* 12-mer and duplex DNA quadruplexes, respectively. Analysis of the thermodynamic parameters obtained from the microcalorimetry study suggests that interactions were most favorable for **BBZ-ARO** among all of the synthesized compounds. The ΔG_{free} obtained from molecular mechanics Poisson−Boltzmann surface area calculations of molecular dynamics (MD) simulation studies suggest that **BBZ-ARO** interacted strongly with G_4-DNA. MD simulation results showed the highest hydrogen bond occupancy and van der Waals interactions were between the side chains of **BBZ-ARO** and the DNA grooves. A significant inhibition of telomerase activity (IC_{50} = 4.56 μM) and induced apoptosis in cancer cell lines by **BBZ-ARO** suggest that this molecule has the potential to be developed as an anticancer agent.

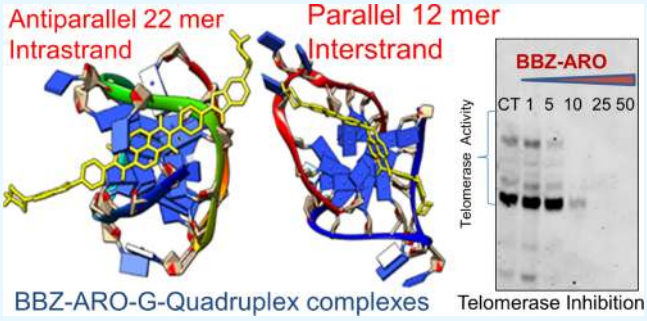

Downloaded via 106.203.38.92 on August 3, 2021 at 10:01:47 (UTC).
See https://pubs.acs.org/sharingguidelines for options on how to legitimately share published articles.

INTRODUCTION

G-quadruplexes are stable secondary structures of nucleic acids (DNA as well as RNA) adapted by guanine-rich sequences, which affect gene regulation, chromatin architecture, and genomic stability.[1−6] Human telomeric DNA has repeated d(TTAGGG) sequences, which cap the ends of chromosomes to protect them during replication from deleterious processes.[7] Telomeres are maintained by telomerase and have been found to be present in tumor cells. It is well known that the formation of a G-quadruplex in telomeres inhibits the telomerase activity and imparts immortality to the cancer cells.[8] Because telomerase is not found in most normal somatic cells, telomeric G-quadraplex stabilization is a strategic approach to inhibit telomerase activity in tumor cells to design anticancer agents.[9−12] A rational design for small molecules targeting DNA G-quadruplexes requires knowledge about the structure of the G-quadruplex and the ligand−quadruplex interaction. Although a number of small molecules have been studied as G-quadruplex-binding ligands, most of them were studied with a prefolded static G-quadruplex; most of the human G-quadruplexes are unstructured dynamic sequences, and except naphthalenediimide (NDI), none of the molecules have reached the in vivo evaluation stage. Hence, a continuous search for small molecules is required for the development of anticancer drugs, which not only induce G-quadruplex formation, but also target different G-quadruplex sequences in human genomes. Considerable efforts have been made to seek effective G-quadruplex binders, such as BRACO-19,[13]

Received: December 19, 2016
Accepted: February 28, 2017
Published: March 16, 2017

 © 2017 American Chemical Society

DOI: 10.1021/acsomega.6b00523
ACS Omega 2017, 2, 966−980

Scheme 1. Reagents and Conditions: (a) $Na_2S_2O_5$, EtOH/H_2O, Reflux 24 h, (b) 10% Pd/C, EtOAc/MeOH (4:1), (c) TFA/DCM, 4 °C for 4 h, (d) Glacial Acetic Acid, Reflux over 8−12 h at 130 °C

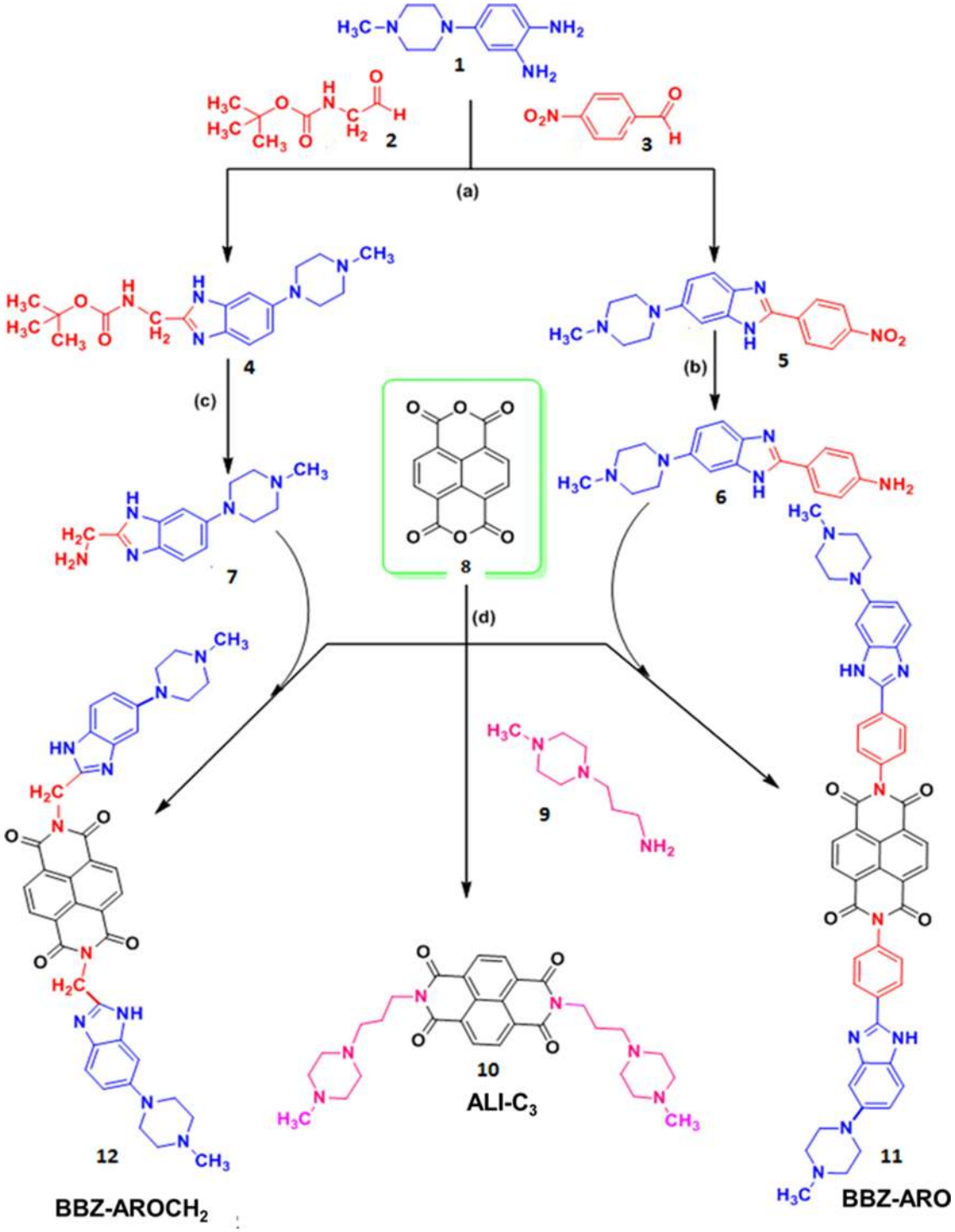

RHPS4,[14] Telomestatin,[15] TMPyP4,[16] and so on, from the library of natural products. Synthetic compounds, such as quinobenzoxazine,[17] coronene,[18] naphthalimide, NDI,[19] isoalloxazine,[20] anthraquinone,[21] spermines,[22] and recently carbazole[23,24] ligands with carboxamide side chains have been shown to be nucleus-imaging probes, which selectively stabilize the c-MYC G-quadruplex. A number of di- and tetrasubstituted derivatives of NDI have been extensively studied for stabilizing the G-quadruplex.[25−27] Four side chains on NDI make its structure too sterically hindered and rigid to bind to quadruplex grooves.[28] Recently, novel NDI derivatives have been found to show anticancer activities.[29,30] Doria et al. synthesized a water-soluble NDI by fusing 1,4-dihydro-pyrazine-2,3-dione with two cationic or anionic chains at the imide moiety.[31] Similarly, quinonemethides were tethered to NDI to convert them to G-quadruplex alkylating agents.[32] An NDI derivative showed antitumor activity in a pancreatic cancer animal model and increased the survival of animals, suggesting in vivo efficacy of G-quadruplex-stabilizing agents.[33]

DOI: 10.1021/acsomega.6b00523
ACS Omega 2017, 2, 966−980

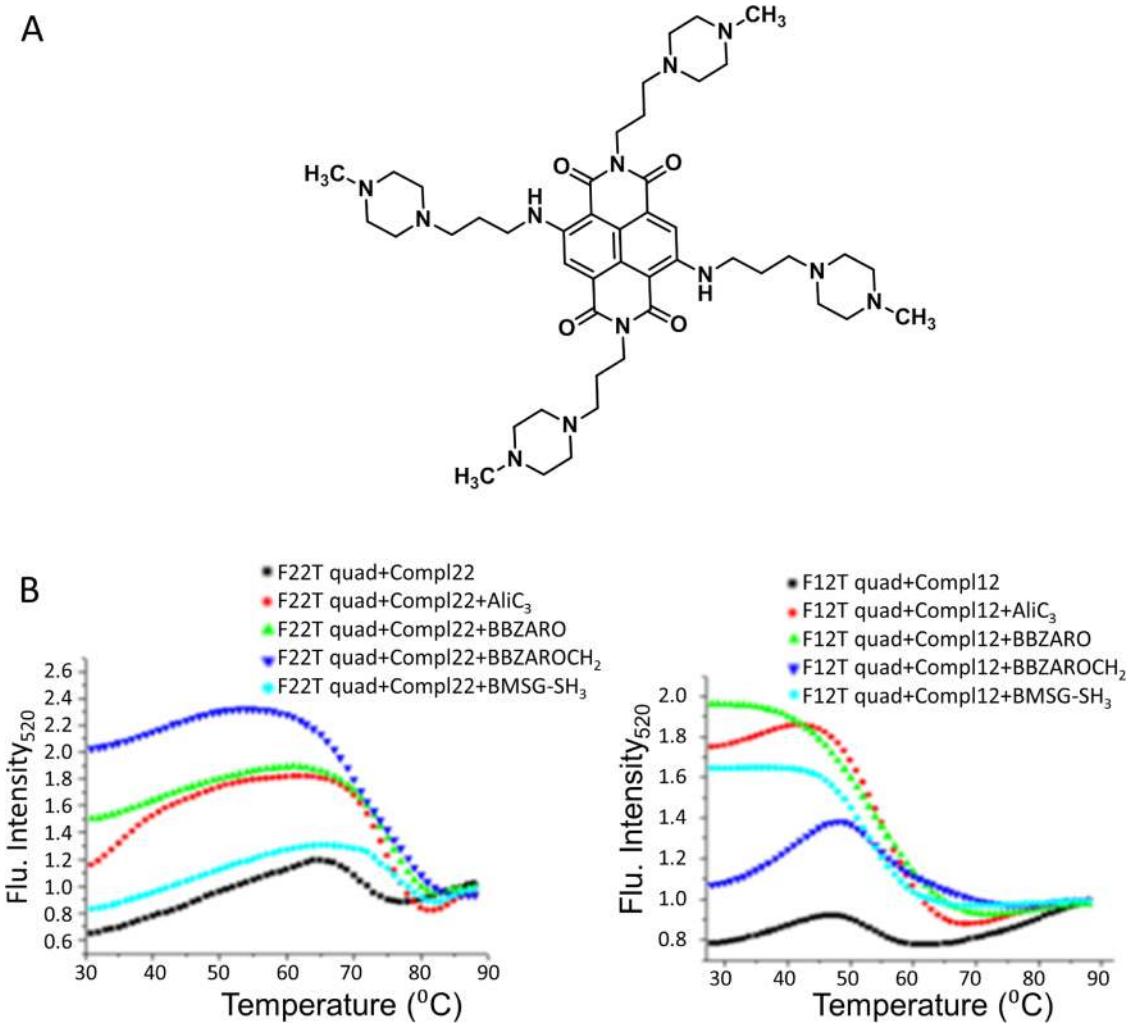

Figure 1. (A) Structure of **BMSG-SH-3**; (B) fluorescence melting temperatures of 5′-fluorescein-AGGGTTAGGGTTA-GGGTTAGGG-3′-TAMRA (F22T) and 5′-fluorescein-TAGGGTTAGG-GT-3′-TAMRA (F12T) with and without competitor complementary DNA sequences; Compl 22:5′-CCCTAACCCTAACCCTAACCCT-3′ and Compl 12:5′-ACCCTAACCCTA-3′, in the presence and absence of ligands.

In the present study, we have designed and synthesized three derivatives of 1,4,5,8-naphthalenetetracarboxylic dimide (NDI) as G-quadruplex-stabilizing ligands; **ALI-C_3 (10)** (2,7-bis(3-(4-methylpiperazin-1-yl)propyl)benzo [*lmn*] [3,8]-phenanthroline-,3,6,8(2*H*,7*H*)-tetraone), **BBZ-ARO (11)** (2,7-bis(4-(6-(4-methyl-piperazin-1-yl)-1*H*-benzo[*d*]imidazol-2-yl)phenyl)-benzo-[*lmn*][3,8] Phenanthroline-1,3,6,8-(2*H*,7*H*)-tetraone), and **BBZ-AROCH$_2$ (12)** (2,7-bis((6-(4-methylpiperazin-1-yl)-1*H*-benzo[*d*]imidazol-2yl)methyl)benzo-[*lmn*][3,8]-phenanthroline-1,3,6,8(2*H*,7*H*)-tetraone) (Scheme 1). Herein, we have studied their interactions with two different quadruplexes, inter-strand 12-mer and an intra-strand 22-mer, and compared the results with those of the parent molecule **BMSG-SH-3** (Figure 1A). **BBZ-ARO** and **BBZ-AROCH$_2$** have a benzimidazole ring along with piperazine in the side chain, whereas **ALI-C_3** has piperazine with three methylenic groups as side chains on two sides of the NDI ring. The molecules synthesized by us showed an increased aromaticity leading to increased end-stacking with G-quadruplex, and the structure with an aliphatic carbon chain provides flexibility to behave as a groove binder. As benzimidazole is structurally isosteric to purine bases, it readily interacts with biomolecules and increases the cell permeability of the ligand.[33] Benzimidazole−carbazole conjugates are reported to have a high binding affinity to G_4-DNA,[34] and the benzimidazole carboxamide derivatives of pyridine, 1,10-phenanthroline and 1,8-naphthyridine, specifically stabilize quadruplex DNA.[35,36]

Our data suggest that, among the three molecules synthesized, **BBZ-ARO** containing bisbenzimidazole side chains is the most potent molecule in terms of affinity toward quadruplex over the duplex DNA. Docking and molecular dynamics (MD) simulations studies were further used for structural insight. We carried out molecular mechanics Poisson−Boltzmann surface area (MM-PBSA) free energy calculations on all of the inter- and intramolecular systems to find out the actual affinities of the ligands and to correlate experimental observations. The therapeutic efficacy was validated by a TRAP-Lig assay, and the cell cycle analysis was validated by flow cytometry and a Annexin V-FITC apoptosis assay.

RESULTS

Synthesis of Bisubstituted NDIs. In the present study, we synthesized an intermediate compound, *N*-4-(4-methylpiperazin-1-yl)-1,2-phenylenediamine (**1**), starting from *m*-chloroaniline, using a reported procedure,[37] and then this intermediate

DOI: 10.1021/acsomega.6b00523
ACS Omega 2017, 2, 966−980

was refluxed with **2** and **3** to produce benzimidazole derivatives **6** and **7**. Compounds **6** and **7** were condensed with 1,4,5,8-naphthalenetetracarboxylic acid anhydride (**8**) to yield **BBZ-ARO** (**11**) and **BBZ-AROCH$_2$** (**12**). We were able to synthesize the tetrasubstituted parent analogue **BMSG-SH-3** (**14**) from 2,6-dibromo-1,4,5,8-naphthalenetetracarboxylic acid dianhydride (**13**) either as a starting amine or heating it at 150 °C for 10 min in a microwave oven. We used 3-(4-methylpiperazin-1-yl) propan-1-amine (**9**) as a starting amine for the synthesis of **ALI-C$_3$** (**10**) from the commercially available intermediate 2,6-dibromo-1,4,5,8-naphthalenetetracarboxylic acid dianhydride (**13**). We could not synthesize **BBZ-ARO** and **BBZ-AROCH$_2$** using **13** because of the degradation of the final product in a microwave oven. To optimize the reaction conditions, different solvents, such as dimethylformamide (DMF), dimethyl sulfoxide (DMSO), ^{i}Pr-OH, and glacial AcOH, were tried for the final step (Scheme 1) of the synthesis of the ligands, but the highest yield was obtained from glacial acetic acid with a formidable 12 h reaction time. We could not isolate the final product by the microwave method, as reported earlier by Neidle et al.[38] The products started to degrade within 10−15 min at 150 W. The solid precipitate was filtered first, washed with glacial acetic acid, and crystallized from DMF/H$_2$O (2:1) and acetic acid separately. The characterization of the compounds using NMR and high-resolution mass spectrometry (HRMS) is described in Figures S1−S26.

Fluorescence Resonance Energy Transfer (FRET) Melting Assay Shows a Strong Binding Preference of BBZ-ARO toward G-Quadruplexes over Duplex DNA. FRET melting results suggest that three ligands display moderate to high stability for human telomeric repeats with G$_4$-conformation. We first monitored by "FAM" and "TAMRA" the melting temperature of a FAM-tagged G-quadruplex (F22T, 5′-[6FAM]-AGGGTTAGGGTTAGGGTTAGGG-[TAM]-3′, and F12T, 5′-[6FAM]-TAGGGTTAGGGT-[TAM]-3′) at increasing concentration of ligand (up to 2 μM) (Figure 1B, Table 1). The FRET melting temperatures were observed as 64.4 and 52.5 °C for F22T and F12T, respectively (Figure S27). There was a slight decrease in the fluorescence intensity in the temperature range of 90−75 °C in the annealing profile of the mixture of G/C-rich strands in the absence of ligands (black curves). However, there was an increase in fluorescence intensities below 75 °C with a subsequent decrease in the temperature (58−37 °C in the case of the F22T-compl 22 system and 48−37 °C in the case of the F12T-compl 12 system). The fluorescence profile of the donor intensity monitored for the mixture of the GC-rich strand in the presence of 2 μM of each ligand shows a shift of the melting profile to a higher temperature. The small change in the fluorescence intensity of the donor in the presence of ligands indicates a lower population of the duplex. The competitive environment caused by the presence of duplex DNA favors quadruplex formation with most ligands, as we found that the melting temperature of F22T increases to 16 from 14 °C in the case of **BBZ-ARO**. The same trends of stability increment were found in the case of F12T and with **ALI-C$_3$** and **BBZ-AROCH$_2$**.

Table 1. Comparative Changes in Melting Temperature (ΔT_m) Determined by FRET Experiments[a]

	ΔT_m (°C)			
entry	F22T	F12T	F22TComp22	F12TComp12
ALI-C$_3$	9 ± 1.2	5 ± 0.8	11 ± 0.6	7 ± 0.5
BBZ-ARO	14 ± 0.5	13 ± 1.4	16 ± 1.6	15 ± 0.5
BBZ-AROCH$_2$	7 ± 0.7	8 ± 0.4	9 ± 0.5	10 ± 1.6
BMSG-SH-3	11 ± 1.3	10 ± 1.5	13 ± 0.9	12 ± 1.7

[a]All data in this table are average of three determinations.

Thermodynamic Parameters Suggest the Highest Binding Affinity of BBZ-ARO with G-Quadruplexes. The interaction of small molecules with macromolecules can be thermodynamically characterized by isothermal titration calorimetry (ITC).[39,40] The appropriate heat values obtained from the injection of the same concentration of ligand solution into the duplex/quadruplex are presented in Figure 2. **ALI-C$_3$**, **BBZ-ARO**, **BBZ-AROCH$_2$**, and **BMSG-SH-3** bound to *h-telo* 22-mer quadruplex exhibited a single binding event. Stoichiometries were found to be 1.06, 1.27, 1.31, and 1.05 for **ALI-C$_3$**, **BBZ-ARO**, **BBZ-AROCH$_2$**, and **BMSG-SH-3**, respectively, suggesting nearly 1:1 binding of the ligand into the complex. **BBZ-ARO** shows the highest affinity of 8.4×10^6 M^{-1} with 22-mer quadruplex. These ligands showed a moderate binding affinity with inter-strand *h-telo* 12-mer quadruplex. **BBZ-ARO** showed the highest binding free energy of −7.59 kcal mol^{-1} among the other synthesized ligands (Table 2). Entropy factors predominate over the enthalpy for **BBZ-ARO**. The control experiments of ligands with duplex DNA showed well-equilibrated isotherms. The binding of ligands with duplex DNA was exothermic in nature. As suggested by the single-site model fitting of ITC data, there was only one binding event for all four ligands. The result yielded a binding affinity of 5.0×10^4 M^{-1} for **BBZ-ARO** with a binding free energy value of −7.86 kcal mol^{-1} with DNA, suggesting that the affinity of the ligand to bind to the duplex is lower compared to that to the quadruplex (Table 2). The ligands **ALI-C$_3$**, **BBZ-AROCH$_2$**, and **BMSG-SH-3**, showed low affinity toward duplex DNA over quadruplexes (Figures 2 and S28). A large enthalpy change ($\Delta H°$) of −15.16 kcal mol^{-1} and a smaller entropy contribution ($T\Delta S°$) of −8.73 kcal mol^{-1} were observed for **BMSG-SH-3** with 22-mer quadruplex. A moderate binding free energy of −7.47 kcal mol^{-1} was observed for **BMSG-SH-3**, which shows effective interaction.

Surface Plasmon Resonance (SPR) Study Validates the Selectivity of Synthesized Compounds toward G-Quadruplex DNA. SPR is a useful technique for the screening of small molecules, to determine their relative binding affinities and selectivity for a target DNA sequence. Concentration-dependent association rate constants were observed, whereas the ligand concentration had no effect on dissociation rate constants. The equilibrium-binding constants (K_A) obtained for the binding of **ALI-C$_3$**, **BBZ-ARO**, **BBZ-AROCH$_2$**, and **BMSG-SH-3** were found to be 8.7×10^6, 9.5×10^7, 1.4×10^6, and 2.7×10^6 M^{-1}, respectively, for *h-telo* 22-mer quadruplex, whereas the corresponding values for the duplex were found to be 0.1×10^6, 0.6×10^6, 0.4×10^6, and 0.8×10^6, respectively. The selectivities of the binding of **ALI-C$_3$** and **BBZ-ARO** with 22-mer quadruplex over DNA duplex as $K_{\text{Ah-telo 22}}/K_{\text{A dsDNA}}$ were found to be 87.0 and 158.3, respectively (Table 3, Figures S29 and S30), proving the stronger binding of ligands with the quadruplex sequence than with the duplex DNA.

BBZ-ARO Binds by End-Stacking to G-Quadruplex. **ALI-C$_3$** binds to the 22-mer quadruplex in a 3′-end by end-stacking mode with G4, G10, G16, and G22 tetrad, and the protonated nitrogen atoms of piperazine, N75 and N79,

DOI: 10.1021/acsomega.6b00523
ACS Omega 2017, 2, 966−980

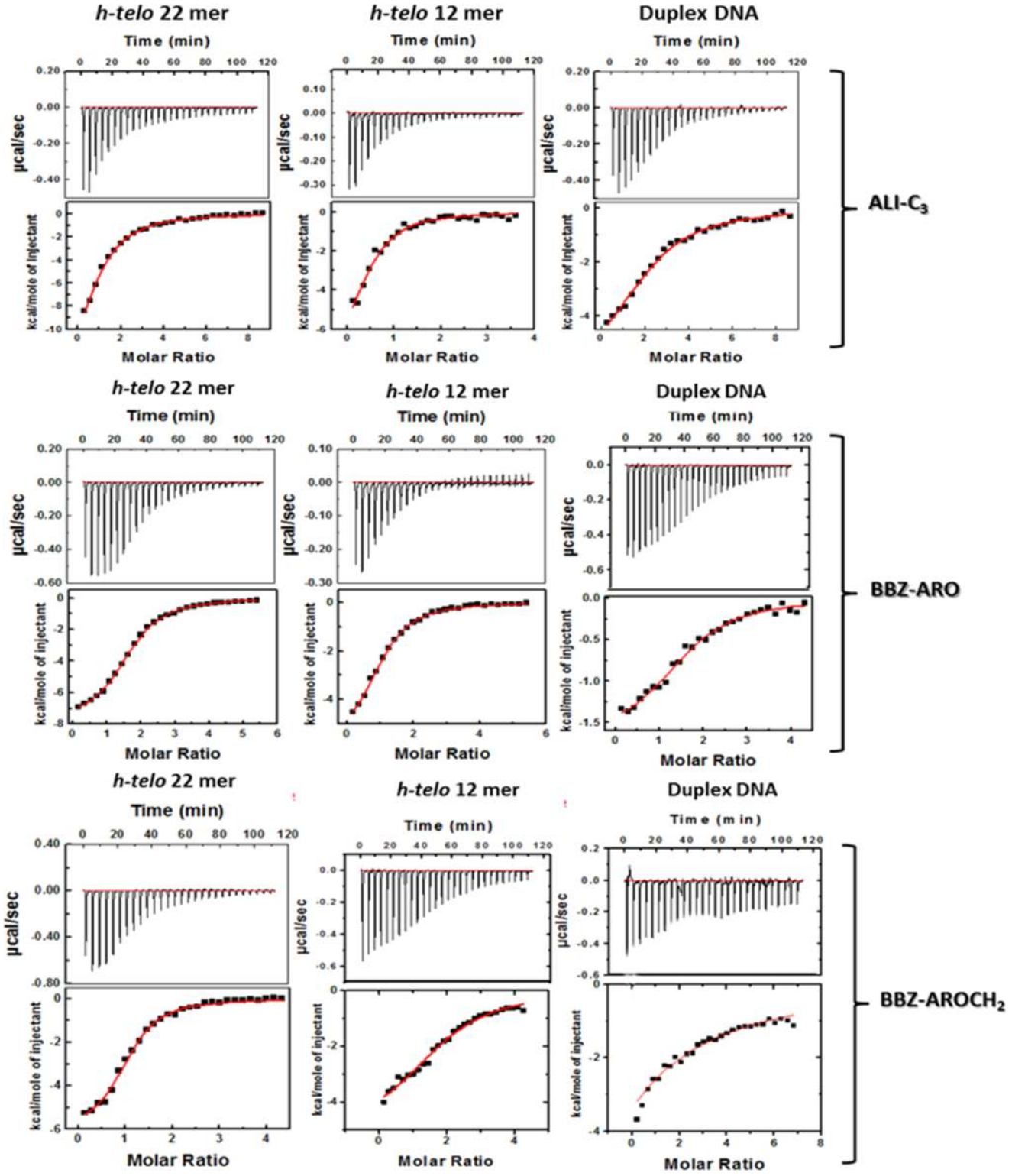

Figure 2. ITC titration profiles of 4×10^{-4} M ligands (**ALI-C$_3$**, **BBZ-ARO**, and **BBZ-AROCH$_2$**) with *h-telo* 22-mer quadruplex (1.0×10^{-5} M), *h-telo* 12-mer quadruplex (0.5×10^{-5} M), and duplex DNA 26-mer quadruplex (1.0×10^{-5} M) at 25 °C.

interacted with the phosphate backbone in the grooves. **BBZ-ARO**, **BBZ-AROCH$_2$**, and **BMSG-SH-3** also bind by an end-stacking mode with the quadruplex, as well as interacting with the phosphate backbone in the grooves depending on the length of the side arms. The GLIDE docking score of **ALI-C$_3$** was observed to be −11.2 (Table S1) with 22-mer G-quadruplex. The flexible side chains of **ALI-C$_3$** allow interaction with quadruplex grooves. However, **BBZ-ARO** shows the best docking score of −12.6 among all four compounds synthesized with 22-mer quadruplex, which can be explained due to the extended aromaticity. However, **BBZ-AROCH$_2$** showed a moderate score of −7.2, as it might lose its planarity because of the absence of a phenyl ring (Figures 3, S31, and S32). The positively charged nitrogen atoms in both side chains in all

DOI: 10.1021/acsomega.6b00523
ACS Omega 2017, 2, 966−980

Table 2. ITC-Derived Thermodynamic Parameters for Intra-Strand 22-mer and Inter-Strand 12-mer G-Quadruplex−Ligand Interaction at 25 °C[a]

ligands	n (drug/target)	binding constant $K_a \times 10^6$ (M^{-1})	$\Delta H°$ (kcal/mol)	$T\Delta S°$ (kcal/(mol K))	$\Delta G°$ (kcal/mol)
		***h-telo* 22-mer**			
ALI-C_3	1.06 ± 0.06	6.35 ± 0.26	−8.73 ± 0.03	−1.07 ± 0.18	−7.66 ± 0.09
BBZ-ARO	1.27 ± 0.05	8.47 ± 0.65	−2.26 ± 0.08	5.54 ± 0.23	−7.81 ± 0.41
BBZ-AROCH$_2$	1.31 ± 0.04	3.41 ± 0.22	−1.28 ± 0.04	6.26 ± 0.08	−7.54 ± 0.15
BMSG-SH-3	1.05 ± 0.03	2.92 ± 0.19	−5.16 ± 1.03	−8.73 ± 0.17	−7.47 ± 0.23
		***h-telo* 12-mer**			
ALI-C_3	0.98 ± 0.11	0.61 ± 1.82	−6.64 ± 0.24	0.76 ± 0.13	−7.41 ± 0.15
BBZ-ARO	1.03 ± 0.19	6.63 ± 2.39	−1.62 ± 0.43	5.97 ± 0.24	−7.59 ± 0.22
BBZ-AROCH$_2$	1.30 ± 0.07	0.89 ± 0.11	−5.13 ± 0.03	2.17 ± 0.03	−7.30 ± 0.17
BMSG-SH-3	1.47 ± 0.04	2.52 ± 1.47	−3.57 ± 0.09	3.52 ± 0.26	−7.09 ± 0.04
	2.36 ± 0.05	6.96 ± 1.18	−5.36 ± 0.02	1.03 ± 0.07	−6.39 ± 0.24
		duplex DNA 26-mer			
ALI-C_3	1.80 ± 0.20	0.03 ± 0.10	−0.71 ± 0.02	6.00 ± 0.12	−6.70 ± 0.03
BBZ-ARO	8.00 ± 0.05	0.05 ± 0.65	−2.26 ± 0.08	5.59 ± 0.01	−7.86 ± 1.06
BBZ-AROCH$_2$	2.49 ± 0.06	0.88 ± 0.63	−2.04 ± 0.02	5.05 ± 0.45	−7.09 ± 0.25
BMSG-SH-3	4.69 ± 0.05	0.04 ± 0.01	−6.67 ± 0.39	0.12 ± 0.18	−6.79 ± 0.37

[a]The reported K_a and $\Delta H°$ values are mean ± SD from three experiments. The values of $\Delta G°$ are determined by $\Delta G° = \Delta H° - T\Delta S°$. All ITC profiles were fit to a model of a single binding site except BMSG-SH-3 with *h-telo* 12-mer quadruplex.

Table 3. SPR Data Showing a Higher Binding Affinity for G-Quadruplex DNA[a]

	h-telo 22-mer			duplex DNA 26-mer			
ligands	K_D (μM)	K_A (M^{-1})	$\Delta G°$ (kcal/mol)	K_D (μM)	K_A (M^{-1})	$\Delta G°$ (kcal/mol)	$K_{A\ h\text{-telo}\ 22}/K_{A\ dsDNA}$
ALI-C_3	0.84	8.7×10^6	−6.95	17.1	0.1×10^6	−6.12	87.0
BBZ-ARO	0.64	9.5×10^7	−8.12	36.6	0.6×10^6	−6.43	158.3
BBZ-AROCH$_2$	0.26	1.4×10^6	−6.14	55.2	0.4×10^6	−6.12	3.5
BMSG-SH-3	0.27	2.7×10^6	−6.37	44.7	0.8×10^6	−6.83	4.3

[a]Error levels for K_A and K_D values were ±15%.

three ligands (specifically in the case of **ALI-C_3**, where the side chains are more flexible because they are aliphatic) targeted the phosphate ions of T5, T11, and T17 of G-quadruplex (in all cases, the phosphate groups of T-residues are interactive). Further, in the case of the 12-mer quadruplex, the two strands mutually form a parallel quadruplex. **BMSG-SH-3** binds by end-stacking with the G5 and G11 of one strand along with G17 and G24 of another strand. Glide docking scores were found to be −8.3 and −9.4 for **ALI-C_3** and **BMSG-SH-3**, respectively. **BBZ-ARO** showed a different binding behavior (docking score −10.4) with the 12-mer quadruplex and lay perpendicular to the G-tetrad, (Figure 3) formed by G5, G11, G17, and G24. The piperazine rings of **BBZ-ARO** interacted with T12 and T24 of the 12-mer quadruplex.

In addition, we performed a flexible docking with Auto Dock Tools to validate the Glide docking results, using the rigid docking protocol. Akin to previous docking, all four ligands showed an end-stacking mode of binding with 22-mer quadruplex and showed similar docking scores.

BBZ-ARO Stabilizes the G-Quadruplex. The MD simulation of all four ligands with the 22-mer intra-strand and the 12-mer inter-strand quadruplexes showed a stable binding of ligands with the quadruplex. There was no dissociation of the ligands from the quadruplex observed for any of the ligand−quadruplex complexes up to 100 ns. The root-mean-square deviations (RMSD) of the ligands, as well as the quadruplexes, are shown in Figure S33. The RMSD of the ligands, as well as the quadruplex, showed a converged (stable) structure throughout the complete time scale except for **BBZ-AROCH$_2$** with 22-mer, which showed a tendency to detach one side chain of **BBZ-AROCH$_2$** during MD. **BBZ-ARO** showed the smallest RMSD (~2 Å) with both quadruplexes due to the high aromaticity, and was followed by the RMSD (2.8 Å) of **ALI-C_3**. The smaller size of **ALI-C_3** helps it to fit appropriately in the binding site in comparison to the size of **BBZ-AROCH$_2$**, **BBZ-ARO**, and **BMSG-SH-3**. Similarly, with the 12-mer quadruplex, the RMSD values were found to be 2.3 ± 0.27 and 1.7 ± 0.52 Å for **BBZ-ARO** and **ALI-C_3**, respectively. The extended chains of **BBZ-AROCH$_2$** are flexible and do not bind tightly to the quadruplex during the dynamics shown in the MD videos in the Supporting Information, which was validated by the RMSD as **BBZ-AROCH$_2$** has mean deviations around 2−3 Å. From the residue-wise root-mean-square fluctuation (RMSF) values, it can be easily perceived that G3, G4, G10, G11, G12, and G22 in the case of 22-mer quadruplex, and G4, T6, G10, T12, T18, and T24 in the case of 12-mer quadruplex, have small residue fluctuations (Figure S34), which might be due to the interactions with corresponding ligands. **BBZ-ARO** showed a higher hydrogen bond occupancy with the 22-mer quadruplex compared to that with the 12-mer quadruplex. Both **ALI-C_3** and **BBZ-AROCH$_2$** showed lower hydrogen bond occupancies with 22-mer and 12-mer quadruplexes compared to those of **BBZ-ARO** (Tables 4 and S2−S4). The comparison of binding sites for two quadruplexes showed different binding cavities. The dynamics of all four ligands during the 100 ns simulations is provided as videos in the Supporting Information. Higher fluctuations of all nucleotides were found in the 22-mer quadruplex with all ligands as compared with those in the 12-mer quadruplex, which was validated by hydrogen bond calculations (Tables S2−S4).

DOI: 10.1021/acsomega.6b00523
ACS Omega 2017, 2, 966−980

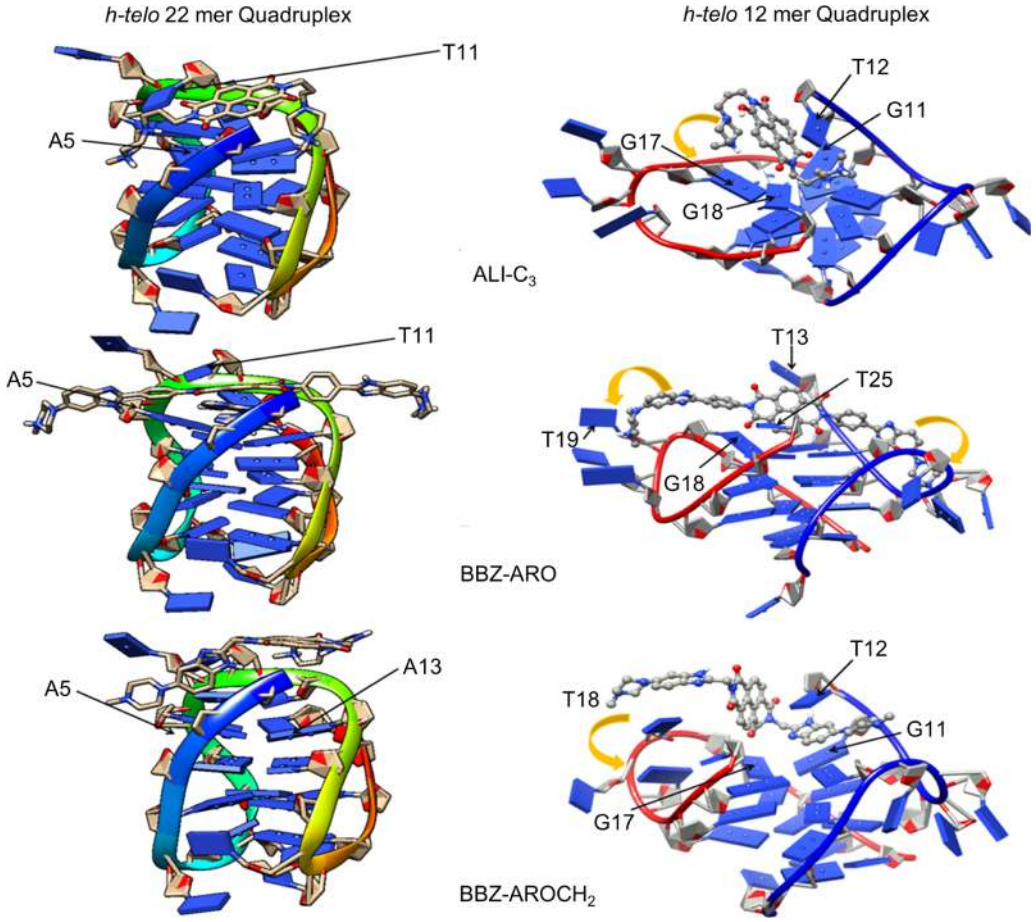

Figure 3. Snapshot of 100 ns simulated ligand−quadruplex complexes; **ALI-C_3**, **BBZ-ARO**, and **BBZ-AROCH$_2$** with *h-telo* 22-mer and *h-telo* 12-mer quadruplexes.

Table 4. Change of Free Energy for Ligands with *h-telo* 22-mer and *h-telo* 12-mer Quadruplexes[a]

ligands	ΔE_{vdw}	ΔE_{ele}	ΔG_{bind}	$T\Delta S$	ΔG_{free}
			h-telo 22-mer		
ALI-C_3	−34.95 ± 3.7	−2025.53 ± 11.2	−36.50 ± 2.1	−25.69 ± 1.9	−10.81 ± 0.3
BBZ-ARO	−62.94 ± 4.6	−746.91 ± 9.2	−39.34 ± 1.9	−23.18 ± 2.1	−16.16 ± 0.2
BBZ-AROCH$_2$	−19.13 ± 1.6	−1001.88 ± 14.2	−15.96 ± 2.1	−8.25 ± 1.2	−07.71 ± 0.9
BMSG-SH-3	−38.24 ± 7.2	−3729.91 ± 19.3	−18.26 ± 4.6	−33.56 ± 4.2	−14.70 ± 0.2
			h-telo 12-mer		
ALI-C_3	−50.78 ± 5.3	−1018.82 ± 10.2	−32.60 ± 2.4	−18.09 ± 1.3	−14.51 ± 1.1
BBZ-ARO	−79.94 ± 6.3	−944.31 ± 9.5	−56.60 ± 3.2	−31.70 ± 2.6	−24.90 ± 0.6
BBZ-AROCH$_2$	−51.73 ± 4.4	4.08 ± 0.2	−35.69 ± 2.1	−29.68 ± 2.6	−06.01 ± 0.4
BMSG-SH-3	−57.21 ± 3.2	−1817.56 ± 11.4	−42.21 ± 4.3	−32.42 ± 6.3	−09.79 ± 2.1

[a]All energies are in kcal mol^{-1}.

Validation of the Stronger Binding of BBZ-ARO with G-Quadruplex over ALI-C_3, BBZ-AROCH$_2$, and BMSG-SH-3 by MD Simulation. The total interactions were calculated using MM-PBSA free energy methods (Tables 4 and 5). It was observed that **BBZ-ARO** binds strongly to the 22-mer quadruplex, and both electrostatic interactions, as well as van der Waals forces, are major contributors. Besides those interactions, the central "NDI" nucleus is involved in the stacking interaction with the G-quartet of the 22-mer quadruplex. **BBZ-ARO** showed stronger van der Waals interactions with less entropic penalties. The quads of bases G2, G3, G4, G10, T11, G15, and G22 are the main nucleotides that participate in the residue interaction map for all four ligands with the 22-mer quadruplex (Table 5). **ALI-C_3** shows a moderate binding with both quadruplexes compared with that of **BBZ-ARO**.

The binding affinity of **BBZ-AROCH$_2$** is moderately high, but it has very small electrostatic interactions, and the van der Waals contribution is the only major factor driving its binding affinity, specifically in the case of the 12-mer quadruplex (Tables 4 and 6). The electrostatic interactions contribute significantly to the total binding affinity of **BMSG-SH-3** with both the 22-mer and 12-mer quadruplexes, making it a strong binder, which is supported by the H-bond scheme (Tables 7 and S4).

DOI: 10.1021/acsomega.6b00523
ACS Omega 2017, 2, 966−980

Table 5. Residue-Wise ΔG_{bind} Contribution of Ligands with *h-telo* 22-mer Quadruplex[a]

residues	ALI-C_3	BBZ-ARO	BBZ-AROCH$_2$	BMSG-SH-3
T1	−12.93	−12.31	−1.20	−5.89
G2		−0.85		−13.84
G3			−3.59	−19.25
G4	−0.48	−0.41		−14.20
T5				−3.73
T6				
A7		−0.01		
G8		−0.01		
G9		−0.32	−0.12	−8.81
G10		−5.21		−1.71
T11	−1.02	−8.92	−0.76	−16.40
G14	−4.87	−5.75	−1.43	−0.55
G15	−1.12	−3.99	−13.44	−0.20
G16	−6.18	−1.23	−6.27	−0.13
T17	−3.89		−0.13	−0.19
G19				
A20		−0.02		
G21		−0.15	−0.12	
G22	−0.10	−0.22	−3.56	−0.22

[a]All energies are in kcal mol^{-1}.

Table 6. Residue-Wise ΔG_{bind} Contribution of Ligands with *h-telo* 12-mer Quadruplex[a]

residues	ALI-C_3	BBZ-ARO	BBZ-AROCH$_2$	BMSG-SH-3
T1				−4.48
A2				−4.63
G3				−2.21
G5	−9.25	−8.56	−6.91	
T6	−3.06	−1.90		
G11	−5.35	−6.73	−6.79	
T12	−14.47	−10.70	−10.00	
T13				−2.81
A14				−10.38
G15				−12.28
G16				−5.37
G17	−3.18	−11.68	−3.37	
T18		−4.72	−12.02	−1.32
T19		−6.58		−6.85
A20		−7.68		−2.40
G21				−8.62
G22		−4.72		
G23	−3.96		−2.44	
T24	−11.16	−10.63	−3.48	

[a]All energies are in kcal mol^{-1}.

A computational study of these ligands with 26-mer duplex DNA was also carried out. After docking of all three ligands, along with **BMSG-SH-3**, followed by 50 ns MD simulation with dsDNA, **ALI-C_3** became completely detached from the duplex, and the other ligands were weakly associated with the duplex; all of the ligands were bound to the major groove of the 26-mer sequence. Comparative RMSD and RMSF profiles, along with the simulated structures and videos of all four ligands, are shown in Figures S35 and S36.

BBZ-ARO Acts as a Potential Telomerase Inhibitor and Is Observed To Be Cytotoxic to Cancer Cells. The TRAP-Lig assay is a sensitive technique that allows telomerase detection, even with a very low telomerase activity. Effective telomerase inhibition was checked by ligand concentration (1−50 μM). A G-quadruplex stabilized by ligands in a TS sequence will inhibit elongation by telomerase and hence there will be a decrease in the ladder intensity. **ALI-C_3** exhibited IC_{50} at >50 μM along with **BBZ-AROCH$_2$**, whereas **BMSG-SH-3** showed inhibition at 25.4 μM. **BBZ-ARO** was observed to be the most potent inhibitor, which inhibits 50% of the telomerase activity at 4.56 μM (Figure 4 and Table 8). **BBZ-ARO** is more toxic to cancerous cells than to near-normal cells. The cytotoxicity of these ligands was determined using methyl thiazolyl tetrazolium (MTT)-based cell survival assay. Mammalian cells HeLa, A549, and HEK293T were treated with increasing concentrations of **ALI-C_3**, **BBZ-ARO**, **BBZ-AROCH$_2$**, and **BMSG-SH-3** for 48 and 72 h (**BMSG-SH-3** used as the reference compound) to analyze ligand toxicity (Table 8 and Figure S37). The IC_{50} values observed for **ALI-C_3** were 1.4, 2.1, and 8.9 μM against A549, HeLa, and HEK293T cells, respectively, after 72 h. **BBZ-ARO** demonstrated values of 19.7, 20.5, and 63.4 μM, whereas **BBZ-AROCH$_2$** showed values of 74.8, 86.5, and >100 μM against A549, HeLa, and HEK293T cell lines, respectively, at 72 h. Reference compound **BMSG-SH-3** showed corresponding values of 6.2, 11.4, and <0.78 μM at 72 h. **BBZ-ARO** displayed a better telomerase inhibition with a considerable toxicity in the cancerous cell line and a lower cytotoxicity in the near-normal HEK293T cells.

BBZ-ARO Causes Cell Cycle Arrest and Apoptosis in Cancer Cell Line. The effect of the ligands on the cell cycle profile of the HeLa cells was evaluated using flow cytometry. Our data revealed that **BBZ-ARO** and **BMSG-SH-3** induced 7.6−15.8 and 21.2% G2/M phase arrest, respectively, as compared to that of the control (Figure 5A). Similarly, **ALI-C3** and **BBZ-AROCH$_2$** showed 7.6−15.7 and 19.1% G2/M phase arrest, respectively, as compared to that of the control. In addition, we also observed cellular accumulation in the sub-G1 phase of the cell cycle fraction (7.3% with **BBZ-ARO** and 2.9% with **BMSG-SH-3**) (Figure 5A), suggesting drug-induced

Table 7. H-Bond Occupancy Table for *h-telo* 22-mer BBZ-ARO and *h-telo* 12-mer BBZ-ARO Complexes

BBZ-ARO *h-telo* 22-mer complex			BBZ-ARO *h-telo* 12-mer complex		
donor	acceptor	occupancy (%)	donor	acceptor	occupancy (%)
G5-side	LIG23-side	27.90	LIG25-side	T18-side	15.99
LIG23-side	T12-side	9.6	LIG25-side	G11-side	1.48
LIG23-side	T11-side	27.20	LIG25-side	G12-side	3.14
LIG23-side	T15-side	10.50	LIG25-side	T6-side	28.06
LIG23-side	G14-side	24.10	LIG25-side	A20-side	1.88
G5-side	LIG23-side	9.20	LIG25-side	G22-side	2.86
T12-side	LIG23-side	40.10			
G14-side	LIG23-side	2.70			

DOI: 10.1021/acsomega.6b00523
ACS Omega 2017, 2, 966−980

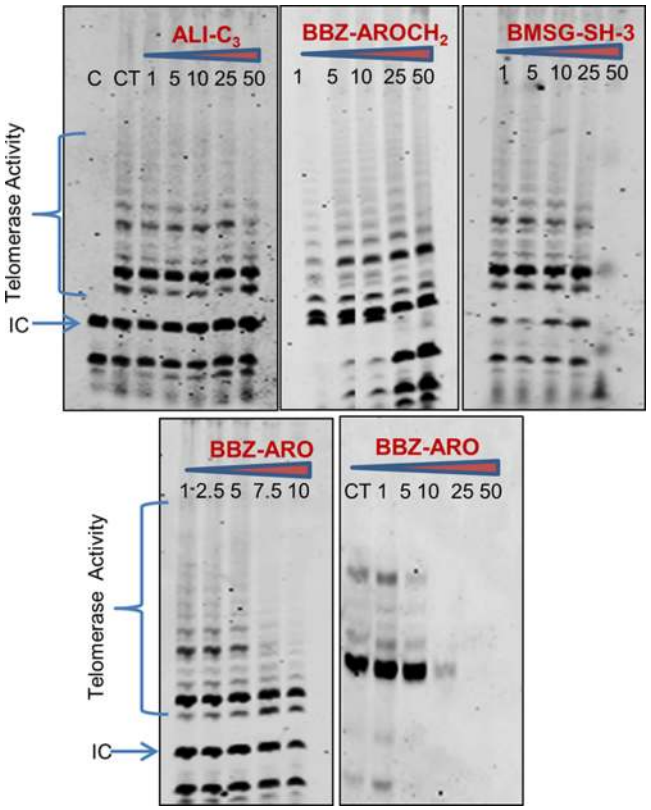

Figure 4. TRAP-Lig assay at increasing concentration of ligands **ALI-C_3**, **BBZ-ARO**, **BBZ-AROCH$_2$**, and **BMSG-SH-3**. The control, C; inactivated telomerase without ligand, CT; with active telomerase but without ligand, 1−50 μM indicates concentration of ligands used to check their effect on enzyme activity; internal control, IC.

apoptosis. However, **ALI-C_3** and **BBZ-AROCH$_2$** did not induce any sub-G1 phase accumulation. Further, the Annexin V assay suggested that **BBZ-ARO** and **BBZ-AROCH$_2$** induced 74 and 40% apoptotic cells, respectively. Similarly, **ALI-C_3** and **BMSG-SH-3** exhibited 35 and 36% Annexin V−FITC positive cells, whereas the control cells did not show any significant evidence of apoptotic cell populations (Figure 5B,C).

DISCUSSION

The present study is the first report of the incorporation of bisbenzimidazoles on NDI moieties as G-quadruplex binders and stabilizers. Here, we have synthesized three molecules with different side-chain lengths to monitor their effect on binding with G-quadruplex DNA as well as duplex DNA (Scheme 1). The rationale for the design of such agents is as follows: (1) benzimidazole, being the isostere of natural purine, will have enhanced interactions with the biopolymer;[41,42] (2) the introduction of aromaticity will provide an increased end-stacking; (3) the positive charge on piperazine increases interactions with the negatively charged phosphate backbone of DNA; and (4) the substitution on two sides of the NDI ring will provide these molecules with a crescent shape, which will contribute to binding with the DNA. The current study was focused on understanding the effect of the two side-chain modifications by increasing the aromaticity and the surface area on stacking with the G-quartet. Our study supports the fact that bisbenzimidazole, which was earlier reported as a DNA minor groove binder, can also bind to G-quadruplexes irrespective of their conformations. Here, we analyzed the FRET melting profile of all ligands, which clearly indicates that these ligands have a preference for quadruplex DNA binding as compared to duplex DNA binding. The ligand-induced stabilization of the quadruplex in the presence of competitor DNA strands suggests that **ALI-C_3**, **BBZ-ARO**, **BBZ-AROCH$_2$**, and **BMSG-SH-3** induce the formation of the G-quadruplex and are selective toward the quadruplex structure over that of duplex DNA. However, when we compare all of the ligands, **BBZ-ARO** appears to be the most potent in terms of the increment of FRET melting in the presence or absence of the complementary DNA sequence. Therefore, the presence of ligands causes a shift in the equilibria toward the formation of quadruplex DNA and not duplex DNA. In addition, we evaluated the effect of all three synthesized ligands on quadruplex stability by studying the thermal melting profiles. Thermal melting was found to be independent of quadruplex concentration, both with and without ligands, indicating the formation of an intramolecular structure (in the case of *h-telo* 22-mer quadruplex). Among all of the ligands, **BBZ-ARO** was observed to show the highest binding affinity and Gibb's binding free energy (ΔG°) when titrated with 12-mer. The reaction was found to be exothermic with a positive entropy and a negative enthalpy. The strong enthalpy contributions make the binding free energy (ΔG°) favorable. The hydrogen bonding and van der Waals interactions between **BBZ-ARO** and **BBZ-AROCH$_2$** with the quadruplex are assumed to contribute to the favorable enthalpy. The large entropic contribution in the case of **BBZ-ARO** suggests a completely different mode of binding from that of the others. **ALI-C_3** and **BMSG-SH-3**, however, showed better enthalpic contributions and negligible entropies, with one and greater than one stoichiometry, respectively. It has been observed in the literature that only intramolecular quadruplexes give accurate results in SPR, as intermolecular quadruplexes undergo a fast regeneration step. Hence, we did not do SPR experiments with 12-mer, which is an intermolecular quadruplex.

The extra phenyl ring in **BBZ-ARO**, purposely placed for the increment of aromaticity as well as for better stacking interactions proved to be the most potent from different experimental data as compared to that of the other counterparts, that is, **BBZ-AROCH$_2$** and **ALI-C_3**. The results from the

Table 8. Determination of Telomerase Enzyme Inhibition Activity through TRAP-LIG Assay and Cytotoxicity of Ligands in Two Cancer Cell Lines (A549 and HeLa) and One Near-Normal (HEK 293T) Cell Line

		A549		HeLa		HEK 293T	
ligands	TRAP assay IC_{50}	IC_{50} at 48 h	IC_{50} at 72 h	IC_{50} at 48 h	IC_{50} at 72 h	IC_{50} at 48 h	IC_{50} at 72 h
ALI-C_3	>50	1.8	1.4	2.4	2.1	12.2	8.9
BBZ-ARO	4.56	26.4	19.7	24.7	20.5	77.9	63.4
BBZ-AROCH$_2$	>50	79.5	74.8	92.7	86.5	>100	>100
BMSG-SH-3	25.4	17.2	6.2	20.9	11.4	<0.78	<0.78

DOI: 10.1021/acsomega.6b00523
ACS Omega 2017, 2, 966−980

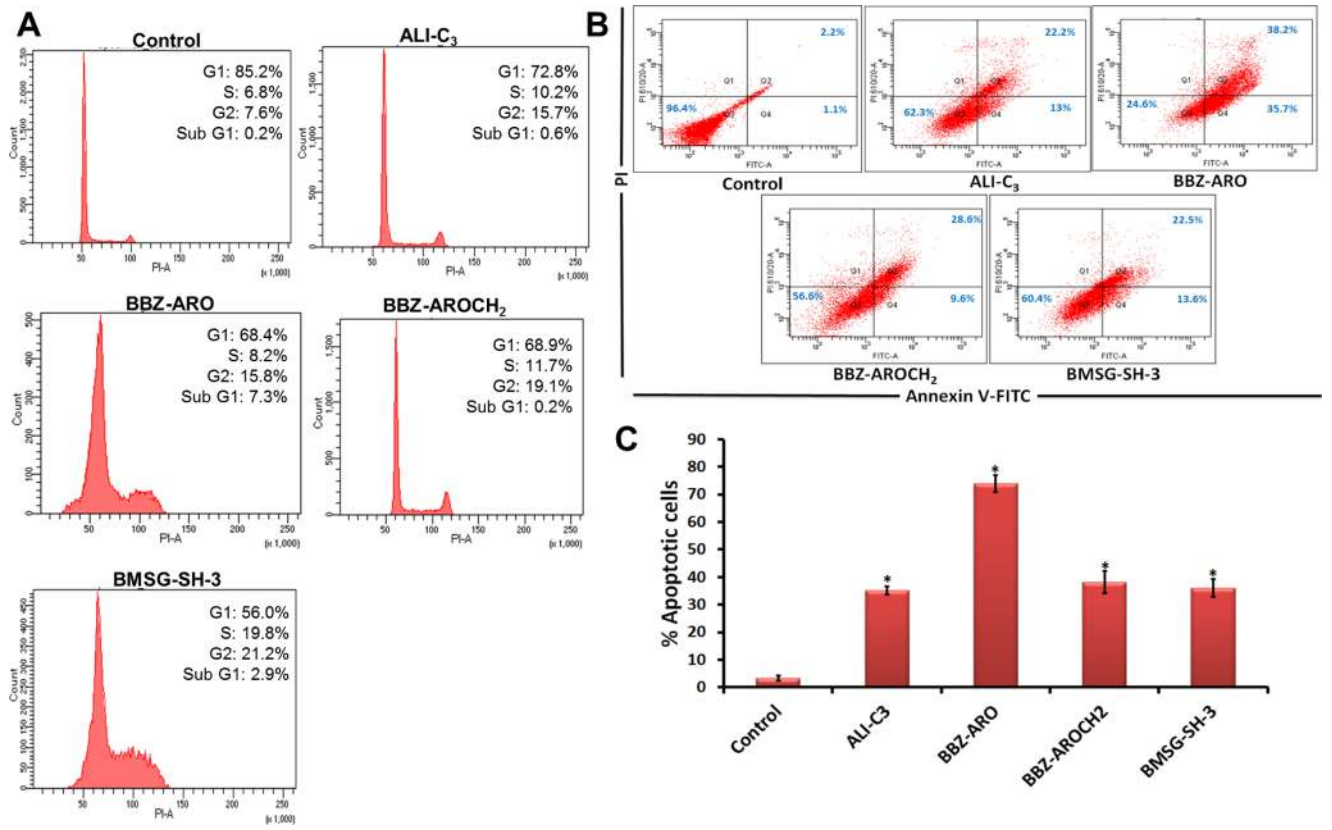

Figure 5. (A) Flow-cytometric cell cycle analysis of HeLa cells treated with 1 μM concentration of different ligands for 24 h. (B) Ligands induce apoptosis after 24 h exposure at 1 μM concentration by Annexin V−FITC labeling in HeLa cells. (C) Bar graph showing quantitative apoptosis by ligand through Annexin V−FITC labeling at 1 μM concentration in HeLa cell line after 24 h. Values are mean ± SEM, *showing statistical significance as compared to that of the control.

different experiments suggest that **BBZ-ARO** binds the most strongly, and stabilizes quadruplex DNA, of the three ligands synthesized. G-quadruplex binding selectivity determined as a fraction of two equilibrium-binding constants (K_{G4DNA}/K_{dsDNA}) was determined by SPR. We also calculated $\Delta G°$ obtained from K ($K = k_{on}/k_{off}$) of the binding from $dG = -RT \ln K$ and compared the values to the free energy values obtained by ITC, and further validated by MD/docking. The MM-PBSA calculations are comparable with the determined thermodynamic parameters and suggest more effective binding of **BBZ-ARO** with quadruplexes as compared to that of **ALI-C$_3$** and **BBZ-AROCH$_2$**. We also suggest that the MM-based free energy computations based on MD simulations are more sensitive for correlating the data obtained from experiments. Thus, the thermodynamic parameters obtained from MD, as well as from docking, can be taken in consideration to conclude that **BBZ-ARO** most effectively binds to both quadruplexes of all of the ligands, in terms of $\Delta G°$. Equilibrium constants obtained from ITC and SPR are not comparable directly as the two techniques follow entirely different principles, but the trends of the results are noticeably comparable. The data obtained showed a similar binding trend with all four ligands and quadruplexes. **BBZ-ARO** displayed the highest inhibition of telomerase activity with considerable ligand-induced toxicity to cancerous cells. The cell cycle experiments showed that **BBZ-ARO** causes G2/M arrest and induces apoptosis in cells. Thus, suggesting **BBZ-ARO** can be further developed as an anticancer agent.

CONCLUSIONS

The introduction of benzimidazole, along with a phenyl side chain, into the scaffold of NDI improved the stability of G-quadruplexes. Replacement of the phenyl ring with a "CH$_2$" group in **BBZ-AROCH$_2$** drastically lowered the stability as compared to that of its aromatic counterpart. Out of the three, **BBZ-ARO** showed the higher preference (>158 times) for the G-quadruplex structure as compared to that of dsDNA. This indicates the association of **BBZ-ARO** with G$_4$-DNA is an entropically driven phenomenon with an intrinsic association constant of the order of 10^6 M^{-1}. ΔE_{vdW} contributed a major part in the stacking of the ligands with the quadruplexes, which was the main reason that **BBZ-ARO** showed the most effective binding with both quadruplexes of the three ligands. The MM-PBSA calculations clearly indicate better effective packing of **BBZ-ARO** with the quadruplexes than that of both **ALI-C$_3$** and **BBZ-AROCH$_2$**. Further, **BBZ-ARO** inhibited telomerase enzyme activity at five times lower concentration as compared to that of the reported **BMSG-SH-3**. **BBZ-ARO** showed less cytotoxicity to near normal cells as compared to cancer cells increasing its therapeutic index. Ligands used in this study help to discriminate G-quadruplex from dsDNA, and further, those ligands have the unique ability to recognize topologically different G-quadruplexes, which can be exploited in their development as anticancer agents.

METHODS

Materials. The ^{1}H (400 MHz) and ^{13}C NMR (100 MHz) spectra were recorded using $CDCl_3$, MeOD, and DMSO-d_6 as

DOI: 10.1021/acsomega.6b00523
ACS Omega 2017, 2, 966−980

the solvent on an ECX-400P, Jeol NMR spectrometer with an internal standard. HRMS spectra were taken using an Agilent 6520 Accurate Mass Q-TOF liquid chromatography/mass spectrometry (LC/MS) mass spectrometer and IR spectra were recorded on a Perkin-Elmer, FTIR system, spectrum BX.

Synthesis. *Tert-Butyl (6-(4-methylpiperazin-1-yl)-1H-benzo[d]imidazol-2-yl)methylcarbamate (**4**).* To the ethanolic solution of the freshly prepared diamine (0.5 g, 1.0 equiv) **1**, a mixture of **2** (*tert*-butyl formyl methylcarbamate, 1.5 equiv) and a solution of $Na_2S_2O_5$ (0.5 equiv) in water (1 mL/100 mg) was added. The resulting solution was stirred at reflux for 24 h, then cooled to room temperature and filtered through a bed of celite. The solvents were evaporated under reduced pressure. The crude residue was found to be the semi-solid title compound. Brown semi-solid; (65% yield, 0.35 g). ^{1}H NMR (400 MHz, $CDCl_3$): δ ppm 1.39 (s, 9H), 2.31 (s, 3H), 2.57 (s, 4H), 3.13 (s, 4H), 4.42 (s, 2H), 5.94 (s, 1H), 6.91−6.93 (m, 2H), 7.24 (d, 1H), 7.41 (s, 1H). ^{13}C NMR (100 MHz, $CDCl_3$): δ ppm 28.2, 38.6, 45.9, 50.8, 55.1, 80.2, 101.3, 114.6, 129.6, 148.2, 151.6, 157.0. Fourier transform infrared (FTIR) (KBr, cm^{-1}): 2929, 1701, 1458, 1284, 1170, 1010. HRMS (ESI): m/z calcd for $C_{18}H_{27}N_5O_2$ $[M + H]^+$ 346.2165 obsd 346.2156. CHN: calcd C 62.58%, H 7.88%, N 20.27%, found C 62.51%, H 7.82%, N 20.41%.

*6-(4-Methylpiperazin-1-yl)-2-(4-nitrophenyl)-1H-benzo[d]-imidazole (**5**).* To the ethanolic solution of the freshly prepared diamine **1** (0.5 g, 1.0 equiv), a mixture of 4-nitrobenzaldehyde **3** (1.5 equiv) and a solution of $Na_2S_2O_5$ (0.5 equiv) in water (1 mL/100 mg) was added. The resulting solution was stirred at reflux for 24 h, then cooled to room temperature and filtered through a bed of celite. The solvents were evaporated under reduced pressure. The crude residue was purified by chromatography on silica gel (100−200 mesh size) in dichloromethane/methanol as the solid title compound. Red solid; (76% yield, 0.38 g); mp 152−154 °C. ^{1}H NMR (400 MHz, MeOD): δ ppm 2.38 (s, 3H), 2.68−2.69 (m, 4H), 3.21−3.22 (m, 4H), 7.01−7.05 (m, 2H), 7.47 (d, J = 8.0 Hz, 1H), 8.09 (d, J = 8.0 Hz, 2H), 8.21 (d, J = 8.0 Hz, 2H). ^{13}C NMR (100 MHz, MeOD): δ ppm 45.7, 49.4, 54.7, 115.4, 117.2, 124.2, 126.7, 136.3, 138.7, 142.4, 147.1, 148.5. FTIR (KBr, cm^{-1}): 3402, 2946, 2823, 1541, 1518, 1345, 855, 797, 707. HRMS (ESI): m/z calcd for $C_{11}H_{16}N_4O_2$ $[M + H]^+$ 338.1539 obsd 338.1586. CHN: calcd C 64.08%, H 5.68%, N 20.76; found C 64.11%, H 5.67%, N 20.4%.

*4-(6-(4-Methylpiperazin-1-yl)-1H-benzo[d]imidazol-2-yl)-benzenamine (**6**).* A solution of compound **5** (1 g, 3 mmol) in ethylacetate: methanol (4:1) was treated with a catalytic amount of 10% Pd/C and the mixture was hydrogenated at room temperature under 40 psi H_2 pressure until thin-layer chromatography showed the disappearance of the starting material and the reaction mixture became colorless. The reaction mixture was filtered through celite. The crude residue was purified by chromatography on silica gel (100−200 mesh size) in dichloromethane/methanol as a solid compound. Dark red solid; (85% yield, 0.85 g); mp 173−176 °C. ^{1}H NMR (400 MHz, DMSO-d_6): δ ppm 2.20 (s, 3H), 2.44−2.48 (m, 4H), 3.05−3,07 (m, 4H), 5.51 (s, 2H), 6.63 (d, J = 8.0 Hz, 2H), 6.82 (dd, J = 8.8, 2 Hz, 2H), 7.42 (s, 1H), 7.76 (d, J = 8.0 Hz, 2H). ^{13}C NMR (100 MHz, DMSO-d_6): δ ppm 45.7, 49.4, 54.7, 115.4, 117.2, 124.2, 126.7, 136.3, 138.7, 142.4, 147.1, 148.5. FTIR (KBr, cm^{-1}): 3442, 3283, 3154, 2944, 2815, 1619, 1247, 1000, 809, 670. HRMS (ESI): m/z calcd for $C_{18}H_{21}N_5$ $[M + H]^+$ 308.1797 obsd 308.1722. CHN: calcd C 70.33%, H 6.89%, N 22.78%; found C 70.31%, H 6.82%, N 22.68%.

*(6-(4-Methylpiperazin-1-yl)-1H-benzo[d]imidazol-2-yl)-methanamine (**7**).* To a solution of **4** in DCM (250 mg, 1.0 equiv), tri-fluoroacetic acid (2.0 equiv. in DCM) was added dropwise over a time period of 1 h. The reaction mixture was kept stirring at 4 °C for 3 h under a N_2 atmosphere. The solvents were evaporated under reduced pressure. The crude residue was purified by chromatography on silica gel (100−200 mesh size) in dichloromethane/methanol as the semi-solid title compound. Brown semi-solid; (58% yield, 0.58 g); ^{1}H NMR (400 MHz, $CDCl_3$): δ ppm 2.48 (s, 2H), 2.87 (s, 3H), 3.02−3.20 (m, 4H), 3.54−3.89 (m, 4H), 4.56 (s, 2H), 7.24 (m, 1H), 7.27 (dd, J = 6.0, 4.0 Hz, 1H), 7.69 (d, J = 9.1 Hz, 1H). ^{13}C NMR (100 MHz, $CDCl_3$-d_6): δ ppm 35.6, 42.0, 47.1, 52.5, 100.8, 114.7, 114.9, 116.0, 118.2, 132.1, 136.9, 147.0. FTIR (KBr, cm^{-1}): 3419, 2254, 2128, 1773, 1690, 1202, 1026. HRMS (ESI): m/z calcd for $C_{13}H_{19}N_5$ $[M + H]^+$ 246.1640 obsd 246.1634. CHN: calcd C 63.65%, H 7.81%, N 28.55%, found C 63.51%, H 7.82%, N 28.41%.

*2,7-Bis(3-(4-methylpiperazin-1-yl)propyl)benzo[lmn][3,8]-phenanthroline-1,3,6,8 (2H,7H)tetraone (**10**).* A mixture of 1-(3-aminopropyl)-4-methylpiperazinecompound **9** (2 mmol) and naphthalene tetracarboxylic dianhydride **8** (0.268 g, 1 mmol) in glacial acetic acid (50 mL) was heated under reflux for 9 h. The obtained solid was filtered off, washed with acetic acid, and crystallized from DMF/H_2O (2:1) and AcOH, respectively, to afford the corresponding final crude product. The crude product was then purified by column chromatography over silica gel (60−120 mesh size) using DCM/MeOH/NH_4OH (9:0.09:0.01) as the mobile phase in quantitative yield of the title compound. Finally, the product was purified by preparative high-performance liquid chromatography (HPLC) as a dark yellowish solid. Brown solid; (33% yield, 0.58 g); mp 225−228 °C. ^{1}H NMR (400 MHz, $CDCl_3$ + TFA-d_4): δ ppm 2.09 (s, 4H), 2.49 (s, 4H), 2.86 (s, 6H), 3.31−3.43 (m, 16H), 4.14 (s, 4H), 8.69 (s, 4H). ^{13}C NMR (100 MHz, $CDCl_3$): δ ppm 24.8, 39.4, 45.9, 52.9, 55.0, 55.9, 119.9, 126.6, 130.8, 162.8. FTIR (KBr, cm^{-1}): 3430, 2934, 2792, 1710, 1657. 1340, 1162, 768, 599. HRMS (ES+) calcd: $C_{30}H_{38}N_6O_4$ $[M + H]^+$ 547.2955. Found: 547.2976. Purity (HPLC, 280 nm): 99.9%. CHN: calcd C 65.91%, H 7.1%, N 15.37%; found C 66.10%, H 6.91% N 15.31%.

*2,7-Bis(4-(6-(4-methylpiperazin-1-yl)-1H-benzo[d]-imidazol-2-yl)phenyl)benzo[lmn][3,8]phenanthroline-1,3,6,8(2H,7H)-tetraone (**11**).* A mixture of compound **6** (2 mmol) and naphthalene tetracarboxylic dianhydride **8** (0.268 g, 1 mmol) in glacial acetic acid (50 mL) was heated under reflux for 12 h. The obtained solid was filtered off, washed with acetic acid, and crystallized from DMF/H_2O (2:1) and AcOH, respectively, to afford the corresponding final crude product. The crude product was then purified by column chromatography over silica gel (60−120 mesh size) using DCM/MeOH/NH_4OH (9:0.09:0.01) as the mobile phase in quantitative yield of the title compound. Finally, the product was purified by preparative HPLC as a dark reddish solid. Brown solid; (30% yield, 0.58 g); mp 212−215 °C. ^{1}H NMR (400 MHz, DMSO-d_6): δ ppm 2.30 (s, 6H), 2.70 (s, 8H), 3.18−3.20 (m, 8H), 3.95 (bs, 2H), 6.98−6.70 (m, 2H), 7.49 (m, 2H), 7.62 (d, J = 8.0 Hz, 2H), 8.04−8.07 (m, 2H), 8.28−8.30 (m, 2H), 8.33−8.35 (m, 2H), 8.40−8.42 (m, 2H), 8.69 (s, 4H). ^{13}C NMR (100 MHz, DMSO-d_6): δ ppm 44.9, 49.1, 54.2, 122.8, 123.3, 125.8, 126.3, 126.6, 126.7, 126.9, 129.7, 130.6, 136.4, 143.8, 147.3,

DOI: 10.1021/acsomega.6b00523
ACS Omega 2017, 2, 966−980

162.9. FTIR (KBr, cm^{-1}): 3400, 2807, 1711, 1668, 1581, 1447, 1347, 1247, 963, 800. HRMS (ES+) calcd.: $C_{50}H_{42}N_{10}O_4$ $[M + 4H]^+$ 850.5875. Found: 850.5881. Purity (HPLC, 280 nm): 90%. CHN: calcd C 70.91%, H 5%, N 16.54%; found C 70.86%, H 4.9%, N 16.5%.

*2,7-Bis((6-(4-methylpiperazin-1-yl)-1H-benzo[d]imidazol-2-yl)methyl)benzo[lmn]-[3,8]-phenanthroline-1,3,6,8-(2H,7H)-tetraone (**12**).* A mixture of compound **7** (2 mmol) and naphthalene tetracarboxylicdianhydride **8** (0.268 g, 1 mmol) in glacial acetic acid (50 mL) was heated under reflux for 12 h. The obtained solid was filtered off, washed with acetic acid, and crystallized from DMF/H_2O (2:1) and AcOH, respectively, to afford the corresponding final crude product. The crude product was then purified by column chromatography over silica gel (60−120 mesh size) using DCM/MeOH/NH_4OH (9:0.09:0.01) as the mobile phase in quantitative yield of the title compound. Finally, the product was purified by preparative HPLC as a dark brownish solid; (26% yield, 0.58 g); mp 268−270 °C. ^{1}H NMR (400 MHz, DMSO-d_6): δ ppm 2.29 (s, 6H), 2.58 (s, 8H), 3.07 (bs, 8H), 3.56 (bs, 2H), 5.44 (s, 4H), 6.83−6.85 (m, 2H), 7.26 (m, 2H), 8.01 (m, 2H), 8.71 (m, 4H). ^{13}C NMR (100 MHz, DMSO-d_6): δ ppm 35.6, 42.0, 47.1, 52.5, 100.8, 114.7, 114.9, 116.0, 118.2, 132.1, 136.9, 139.8, 147.0, 149.9, 159.1. FTIR (KBr, cm^{-1}): 3400, 2927, 1702, 1670, 1458, 1113, 773, 618. HRMS (ES+) calcd: $C_{41}H_{40}N_{10}O_5$ $[M + 2H]^+$ 724.3077. Found: 724.3122. Purity (HPLC, 280 nm): 70%. CHN: calcd C 66.47%, H 5.30%, N 10.38%; found C 66.46%, H 5.2% N 10.1%.

Compound purity was determined through analytical HPLC using a Dionex Ultimate 3000 controlled using a YMC ODS-AQ analytical column (4.6 mm × 250 mm) and a Dionex ultimate 3000 photo diode array detector around 340 nm wavelength. Acetonitrile/water with 0.1% formic acid was used as the solvent system with a gradient mode at 1 mL/min flow rate for HPLC analysis (the detailed procedure is described in Supporting Information). Compounds were found to be more than 95% pure on HPLC analysis.

Sample Preparation. Throughout the study, we used three oligomeric HPLC purified DNA sequences; human telomeric 22-mer sequence (*h-telo* 22-mer quadruplex) 5′-AGGGT-TAGGG-TTAGGGTTAGGG-3′, 12-mer inter-strand forming quadruplex sequence (*h-telo 12-mer*) 5′-TAGGGTTAGGGT-3′, and self-complementary duplex sequence (26-mer duplex DNA) 5′-CAATCGGATCGAATTCGATCCGATTG-3′ as the positive control, purchased from Sigma-Aldrich, Singapore. The molar absorption coefficient values used for the 22-mer and 12-mer oligonucleotide sequences d(AGGGTTAGGG-TTAGGGTTAGGG) were obtained from equally concentrated solutions of the monomers in buffer solution (10 mM sodium cacodylate, 0.5 mM EDTA, and 25 mM KCl, pH 7.0), heated to 95 °C for 10 min and then cooled gradually to 4 °C. Ligand stock solutions were made with a working buffer solution and their concentration was determined spectroscopically in cuvettes of 1 cm path length using the molar absorption coefficients (M^{-1} cm^{-1}): 285 000 at 362 nm for **ALI-C_3**; 256 270 at 350 nm for **BBZ-ARO**; 238 000 at 360 nm for **BBZ-AROCH$_2$**; 244 950 at 369 nm for **BMSG-SH-3**. Freshly prepared working stock solutions were used beforehand. We used the same (above mentioned) buffer throughout all our experiments except the SPR study.

FRET Experiments of G-Quadruplexes with Ligands in the Presence of Duplex DNA. HPLC purified dual-labeled G-rich oligonucleotides (5′-fluorescein and 3′-TAMRA) and their respective unlabeled complementary strands were purchased from Sigma-Aldrich, India, for fluorescence melting experiments. 5′-Fluorescein-TAGGGTTAGGGT-3′-TAMRA (F12T) and 5′-fluorescein-AGGGTTAGGGTTAGGGT-TAGGG-3′-TAMRA (F22T) were used for fluorescence experiments conducted in a Cary Eclipse Spectrofluorimeter at constant temperature with the help of peltier. Both oligos were prepared by incubating F22T and F12T quadruplex forming strands (0.25 μM) with their respective 10 times high concentration of complementary unlabeled single strand (2 μM) for 24 h at 25 °C. The different melting experiments were performed with or without 2 μM concentrations of each ligand (**ALI-C_3**, **BBZ-ARO**, and **BBZ-AROCH$_2$**) in buffer solutions with both quadruplex samples mentioned above. The fluorescein signal at 520 nm was analyzed as described earlier.[43−47] Fluorescence emission at 520 nm was recorded with excitation at 480 nm at 1 °C intervals from 25−95 °C and 60 s was set for sample optimization prior to each reading to ensure stabilization. G-quadruplex melting was monitored with or without varying concentrations of the ligands and/or of the single stranded competitor Compl 22 (5′-CCCTAACC CTAACCCTAACCCT-3′) and Compl 12 (5′-AC-CCTAACCCTA-3′). Data analysis was performed in Origin 7.5.

ITC of Ligands with G-Quadruplexes. ITC experiments[48] were done on a Microcal VP-ITC unit (MicroCal, Inc., Northampton, MA). The energetics of the binding of the synthesized ligands **ALI-C_3**, **BBZ-ARO**, **BBZ-AROCH$_2$**, and **BMSG-SH-3** with *h-telo* 22-mer intra-strand quadruplex and *h-telo* 12-mer inter-strand quadruplex, along with the control duplex DNA, were carried out in the same buffer at pH 7.0 at 25 °C. Microcal's Thermovac unit was used to degas all solutions under vacuum (160 mbar, 10 min) prior to use. Approximate aliquots of 5−10 μL of the ligands (4×10^{-4} M) were injected from a rotating (381 rpm) micro syringe into the 1.4235 mL calorimeter cell containing the DNA quadruplex and duplex solution (1.0×10^{-5} M) to achieve a binding isotherm completely. The duration was taken as 20 s; 240 s was fixed as the delay time between each injection, and the initial delay was kept as 60 s before the first injection throughout the experiments. A heat burst curve (microcalories against time) was obtained with the area under the peak determined from integration of the measured heat associated with each injection (Origin 7.0 software). Thermograms derived from the difference of experimental heat from the corresponding heat associated with the ligand−DNA injection were studied by the single binding site model of the Levenberg−Marquardt nonlinear least squares curve fitting algorithm.

A similar ligand concentration in the buffer at the same volume was used to perform control experiment to generate the heat of ligand dilution. Similarly, experimental heat of ligand dilution was subtracted from the reaction generated heat and this corrected injection heat was plotted as a function of molar ratio. Micro Cal Origin software was used to fit titration curves with the assumption of a single binding site. Free energy change (ΔG°) and entropy (ΔS°) were calculated from the relationship $\Delta G^\circ = -RT \ln K_a = \Delta H^\circ - T\Delta S^\circ$. The reported K_a and ΔH° values are mean ± standard deviation (SD) from three experiments.

SPR Studies of Ligands with G-Quadruplexes. SPR measurements were performed on Streptavidin-coated sensor chips (Sensor chip SA, BIAcore Inc.)[48] in BIAcore 3000 (BIAcore Inc.). All 5′-biotinylated sequences containing T9

DOI: 10.1021/acsomega.6b00523
ACS Omega 2017, 2, 966−980

linker (Btn-TTTTTTTTT-5′-AGGGTT-AGGGTTAGGGT-TAGGG-3′ and Btn-TTTTTTTTT-5′-CAATCGGAT-CGAATTC-GATCCGATTG-3′) were heated to 95 °C and allowed to anneal to form a quadruplex by gradual cooling in 10 mM HEPES buffer containing 100 mM KCl with 0.005% surfactant IGEPAL (pH 7.4). The immobilized oligonucleotide surface was equilibrated with running buffer for 2 h at 20 μL/min flow rate at 25 °C. Different analyte concentration solutions (1.0×10^{-9} to 10^{-6} M) in running buffer were injected for 300 s at the same flow rate randomly to overcome systematic error. 1 M NaCl in 50 mM NaOH was used for regeneration. Binding sensorgrams by a two independent binding site model were analyzed by BIA evaluation software 3.1. All experiments were conducted in triplicate and values are mean ± standard error (SEM).

Molecular Docking Protocol. The initial structures for intra-strand G-quadruplex DNA (PDB accession code: 143D)[49] and inter-strand G-quadruplex DNA (PDB accession code: 1K8P)[50] were taken from the protein data bank. All four ligands, **ALI-C_3**, **BBZ-ARO**, **BBZ-AROCH$_2$**, and **BMSG-SH-3**, were docked in 22-mer and 12-mer G-quadruplexes using Glide v 5.7. Ligands were prepared by the Ligprep module and quadruplexes were minimized using an Amber force field implemented in Schrodinger suits. A grid with dimensions of $50.10 \times 48.63 \times 40.56$ Å^3 over the G-quadruplex was used. The defined grid covers the entire topology of the G-quadruplex so that the ligand position and orientation relative to the receptor can be sampled sufficiently; the conformation of the receptor was also fixed during the docking. The standard precision mode of the software was used for the initial screening of the molecules. Selected top scoring molecules binding to the desired core of the G-quadruplex were selected for the extra precision mode of docking. Glide uses rigid docking protocol; therefore, to account for the conformational dynamics during docking, we used AutoDock4 in addition to Glide. We used standard protocol for receptor grid generation and ligand docking in Auto docks tools.[51]The best docking pose, ranked according to docking scores, was selected for further MD simulations study.[52−54]

MD Simulations. We used Amber 14[55] for all MD simulations and free energy calculations. As the parameters for the ligands were not present in the Amber library, therefore parameters for all ligands were prepared by the antechamber module. HF/6-31 G* level of theory was taken for ab initio calculation from Gaussian 03 and calculation of partial charges were done by the restraint electrostatic potential method. The whole system was neutralized with K^+ ions and taken into a rectangular box of TIP3P water extending over 10.0 Å from the quadruplex exterior. Ptraj module of Amber14 was used for post MD analysis. VMD 1.6.7 was used to perform analysis of trajectories,[56] whereas trajectory visualization was done using Chimera-1.5[57] and Maestro[58] graphical programs. The analysis of free energy from the production trajectories using the single trajectory MM-PBSA approach was used.[59,60] The free energy difference of binding was measured with the following equation

$$\Delta G_{\text{free}} = \Delta G_{\text{electrostatic}} + \Delta G_{\text{vdW}} + \Delta G_{\text{polar}} + \Delta G_{\text{nonpolar}} - T\Delta S$$

where ΔG and ΔH are the binding free energy and enthalpy change at temperature T, respectively.

Determination of Inhibition of Cellular Telomerase Activity Using TRAP-Lig Assay. The TRAP-Lig assay was performed as reported earlier from A549 cells.[41,42] Briefly, 1 00 000 cells were collected and lysed in a 100 μL ice-cold NP-40 lysis buffer. After 30 min incubation, the supernatant was collected for the TRAP-Lig assay. 0.5 μL of this supernatant was treated with increasing concentrations of ligands (1, 5, 10, 25, 50 μM). Each reaction tube contained 50 μM final concentrations of the dNTP mix, 1× TRAP buffer, 20 μg of final concentration ultrapure bovine serum albumin (BSA), 200 ng of the TS primer (5′-Cy3-AATCCGTCGAGCAGAGTT, HPLC purified), and 1 μL of the primer mix recipe mentioned below was further added for each sample.

The final 50 μL reaction volume was achieved adding RNase-free water. Primer mix content: 10 μg of each ACX primer: 5′-GCGCGGCTTACCCTTACCCTT-ACCCTAACC-3′ and NT primer: 5′-ATCGCTTCTCGGCCTTTT-3′ and 1 μL (TSNT oligonucleotide: 5′-AATC-CGTCGAGCAGAGT-TAAAAGGCCGAGAAGCGAT-3′ diluted to final concentration up to 1.0×10^{-18} mol μL^{-1}) was mixed and the volume made up to 100 μL by adding RNase-free water. After 30 min incubation at 37 °C, telomerase extension products were column purified (QIA quick nucleotide purification kit, Qiagen). Purified telomerase extended samples were mixed with equal volumes of the master mix containing 1 μL of the primer mix, 200 ng of the TS primer, TRAP buffer, 20 μg of BSA final concentration, 50 μM dNTPs (final concentration) and equal Taq polymerase. Samples were amplified as per reported polymerase chain reaction conditions. Subsequent amplification yielded a 6-bp incremental ladder, which was further analyzed by 10% w/v nondenaturing polyacrylamide gel electrophoresis in 0.5× TBE. The gel was then fixed in 50% ethanol for 30 min and scanned under Cy3 (green) fluorescence with a phosphorimager.

In Vitro Cell Proliferation Assay. Human cervical (HeLa), lung adenocarcinoma epithelial (A-549), and human embryonic kidney (HEK 293T) cells were obtained from the National Center for Cell Science, Pune, India. After 48 and 72 h incubation with **ALI-C_3**, **BBZ-ARO**, and **BBZ-AROCH$_2$** at 37 °C, the ligand containing medium was replaced with 200 μL of fresh medium with equal MTT reagent and incubated for 4 h. The formazon product was dissolved in equal volumes of DMSO and the samples were read at 570 nm using a microplate reader (Infinite M 200, Tecan, Singapore).

Annexin V-FITC/PI Staining. Ligand mediated apoptosis in HeLa cells was studied by Annexin V-FITC/PI Staining following the manufacturer's guidelines (V13242, Invitrogen, Life technology, India). Briefly, 2×10^5 cells per 60 mm plate were treated with indicated ligands at 1 μM concentration. Cells were collected after 24 h, washed through PBS twice and resuspended in the provided buffer at a final concentration of 1×10^6 cells/mL. Equal volumes of Annexin V-FITC were added to all samples, mixed well, and further incubated for 15 min in the dark at room temperature. The final volume was achieved with a binding buffer and samples were analyzed on LSR II (Becton Dickinson).

Cell Cycle Analysis by Flow Cytometry. Cell cycle analysis by flow cytometry was carried out as described in the literature[61] with minor modifications. Briefly, subconfluent HeLa cells were treated with indicated ligands at 1 μM concentration for 24 h. Cells were collected, washed twice with PBS, and fixed in chilled 70% ethanol. Subsequently, cells were treated with RNAse (0.5 mg/mL) and then stained with propidium iodide (50 μg/mL). Acquisition was done on a

DOI: 10.1021/acsomega.6b00523
ACS Omega 2017, 2, 966−980

FACS BD LSR Fortessa and analyzed using BD FACS Diva software.

■ ASSOCIATED CONTENT

Supporting Information

The Supporting Information is available free of charge on the ACS Publications website at DOI: 10.1021/acsomega.6b00523.

Synthesis procedure (compound **1**, **13**−**14**), HPLC method, ^{1}H NMR, ^{13}C NMR and mass data, docking poses of ligands, docking scores table, hydrogen bond occupancy tables, UV melting profiles, fluorescence melting profiles, ITC titration profiles, SPR profiles with quadruplexes and dsDNA (PDF)

Dynamics of the four ligands under study (MPG) (MPG) (MPG) (MPG) (MPG) (MPG) (MPG) (MPG) (MPG) (MPG) (MPG) (MPG)

■ AUTHOR INFORMATION

Corresponding Author

*E-mail: vtandon@mail.jnu.ac.in, vtandon@acbr.du.ac.in. Phone: 91-11-26741640; 91-11-26708783.

ORCID

Gopinatha Suresh Kumar: 0000-0002-3596-979X

Vibha Tandon: 0000-0001-6146-937X

Author Contributions

⊥S.S., V.Ti., and D.S. equally contributed to this work.

Author Contributions

All authors contributed in writing this manuscript and approved its final version as well.

Notes

The authors declare no competing financial interest.

■ ACKNOWLEDGMENTS

S.S. and V.Ti. are thankful to the Council of Scientific & Industrial Research (CSIR) and D.S. is thankful to the Indian Council for Medical Research (ICMR) for providing a fellowship as Senior Research Fellow. M.Z.K. is supported by DSK postdoctoral fellowship. We want to acknowledge Dr. Souvik Maiti, CSIR-IGIB, Delhi, for his valuable suggestions and USIC, DU & AIRF, and JNU for providing instrumentation facilities. We are also thankful to BRAF-CDAC, Pune, India, for providing the Computational facility. UGC, DST, DU, and JNU (DST PURSE, UPOE-II grant) New Delhi, India, supported by funding the present work.

■ REFERENCES

(1) Rodriguez, R.; Miller, K. M. Unravelling the genomic targets of small molecules using high-throughput sequencing. *Nat. Rev. Genet.* **2014**, *15*, 783−796.

(2) Wolfe, A. L.; Singh, K.; Zhong, Y.; Drewe; Rajasekhar, V. K.; Sanghvi, V. R.; Mavrakis, K. J.; Jiang, M.; Roderick, J. E.; Van der Meulen, J.; Schatz, J. H.; Rodrigo, C. M.; Zhao, C.; Rondou, P.; de Stanchina, E.; Teruya-Feldstein, J.; Kelliher, M. A.; Speleman, F.; Porco, J. A., Jr.; Pelletier, J.; Rätsch, G.; Wendel, H. G. RNA G-quadruplexes cause eIF4A-dependent oncogene translation in cancer. *Nature* **2014**, *513*, 65−70.

(3) Maizels, N. Genomic stability: FANCJ-dependent G4 DNA repair. *Curr. Biol.* **2008**, *18*, R613−R614.

(4) Haeusler, A. R.; Donnelly, C. J.; Periz, G.; Simko, E. A.; Shaw, P. G.; Kim, M. S.; Maragakis, N. J.; Troncoso, J. C.; Pandey, A.; Sattler, R.; Rothstein, J. D.; Wang, J. C9orf72 nucleotide repeat structures initiate molecular cascades of disease. *Nature* **2014**, *507*, 195−200.

(5) Bugaut, A.; Balasubramanian, S. 5′-UTR RNA G-quadruplexes: translation regulation and targeting. *Nucleic Acids Res.* **2012**, *40*, 4727−4741.

(6) Kumari, S.; Bugaut, A.; Huppert, J. L.; Balasubramanian, S. An RNA G-quadruplex in the 5′ UTR of the NRAS proto-oncogene modulates translation. *Nat. Chem. Biol.* **2007**, *3*, 218−221.

(7) Blackburn, E. H. Structure and Function of Telomeres. *Nature* **1991**, *350*, 569−573.

(8) Kelland, L. R. Telomerase inhibitors: targeting the vulnerable end of cancer? *Anticancer Drugs* **2000**, *11*, 503−513.

(9) Nugent, C. I.; Lundblad, V. The telomerase reverse transcriptase: components and regulation. *Genes Dev.* **1998**, *12*, 1073−1085.

(10) Neidle, S. Human telomeric G-quadruplex: the current status of telomeric G-quadruplexes as therapeutic targets in human cancer. *FEBS J.* **2010**, *277*, 1118−1125.

(11) Neidle, S.; Parkinson, G. Telomere maintenance as a target for anticancer drug discovery. *Nat. Rev. Drug Discovery* **2002**, *1*, 383−393.

(12) Shinohara, K.; Sannohe, Y.; Kaieda, S.; Tanaka, K.; Osuga, H.; Tahara, H.; Xu, Y.; Kawase, T.; Bando, T.; Sugiyama, H. A Chiral Wedge Molecule Inhibits Telomerase Activity. *J. Am. Chem. Soc.* **2010**, *132*, 3778−3782.

(13) Burger, A. M.; Dai, F.; Schultes, C. M.; Reszka, A. P.; Moore, M. J.; Double, J. A.; Neidle, S. The G-quadruplex-Interactive Molecule BRACO-19 Inhibits Tumor Growth, Consistent with Telomere Targeting and Interference with Telomerase Function. *Cancer Res.* **2005**, *65*, 1489−1496.

(14) Phatak, P.; Cookson, J. C.; Dai, F.; Smith, V.; Gartenhaus, R. B.; Stevens, M. F.; Burger, A. M. Telomere Uncapping by the G-quadruplex Ligand RHPS4 Inhibits Clonogenic Tumour Cell Growth in vitro and in vivo consistent with a Cancer Stem Cell Targeting Mechanism. *Br. J. Cancer* **2007**, *96*, 1223−1233.

(15) Shin-ya, K.; Wierzba, K.; Matsuo, K.; Ohtani, T.; Yamada, Y.; Furihata, K.; Hayakawa, Y.; Seto, H. Telomestatin, a Novel Telomerase Inhibitor from *Streptomyces anulatus*. *J. Am. Chem. Soc.* **2001**, *123*, 1262−1263.

(16) Fiel, R. J.; Howard, J. C.; Mark, E. H.; Datta, G. N. Interaction of DNA with a Porphyrin Ligand: Evidence for Intercalation. *Nucleic Acids Res.* **1979**, *6*, 3093−3118.

(17) Mehta, A. K.; Shayo, Y.; Vankayalapati, H.; Hurley, L. H.; Schaefer, J. Structure of a Quinobenzoxazine-G-quadruplex Complex by REDOR NMR. *Biochemistry* **2004**, *43*, 11953−11958.

(18) Diev, V. V.; Schlenker, C. W.; Hanson, K.; Zhong, Q.; Zimmerman, J. D.; Forrest, S. R.; Thompson, M. E. Porphyrins Fused with Unactivated Polycyclic Aromatic Hydrocarbons. *J. Org. Chem.* **2012**, *77*, 143−159.

(19) Hampel, S. M.; Pepe, A.; Greulich-Bode, K. M.; Malhotra, S. V.; Reszka, A. P.; Veith, S.; Boukamp, P.; Neidle, S. Mechanism of the Antiproliferative Activity of Some Naphthalene Diimide G-quadruplex Ligands. *Mol. Pharmacol.* **2013**, *83*, 470−480.

(20) Balasubramanian, R.; Raghavan, B.; Steele, J. C.; Sackett, D. L.; Fecik, R. A. Tubulysin Analogs Incorporating Desmethyl and Dimethyl Tubuphenylalanine Derivatives. *Bioorg. Med. Chem. Lett.* **2008**, *18*, 2996−2999.

(21) Kintzer, A. F.; Thoren, K. L.; Sterling, H. J.; Dong, K. C.; Feld, G. K.; Tang, I. I.; Zhang, T. T.; Williams, E. R.; Berger, J. M.; Krantz, B. A. The Protective Antigen Component of Anthrax Toxin forms Functional Octameric Complexes. *J. Mol. Biol.* **2009**, *392*, 614−629.

(22) Kabir, A.; Kumar, G. S. Targeting Double-Stranded RNA with Spermine, 1-naphthylacetyl spermine and Spermidine: A Comparative Biophysical Investigation. *J. Phys. Chem. B* **2014**, *118*, 11050−11064.

(23) Cuenca, F.; Greciano, O.; Gunaratnam, M.; Haider, S.; Munnur, D.; Nanjunda, R.; Wilson, W. D.; Neidle, S. Tri- and tetra-substituted naphthalene diimides as potent G-quadruplex ligands. *Bioorg. Med. Chem. Lett.* **2008**, *18*, 1668−1673.

(24) Debnath, M.; et al. Small molecule regulated dynamic structural changes of human G-quadruplexes. *Chem. Sci.* **2016**, *7*, 3279−3285.

(25) Suseela, Y. V.; Das, S.; Pati, S. K.; Govindaraju, T. Imidazolyl-Naphthalenediimide-Based Threading Intercalators of DNA. *ChemBioChem* **2016**, *17*, 2162−2171.

(26) Panda, D.; Debnath, M.; Mandal, S.; Bessi, I.; Schwalbe, H.; Dash, J. A Nucleus-Imaging Probe That Selectively Stabilizes a Minor Conformation of c-MYC G-quadruplex and Down-regulates c-MYC Transcription in Human Cancer Cells. *Sci. Rep.* **2015**, *5*, No. 13183.
(27) Collie, G. W.; Promontorio, R.; Hampel, S. M.; Micco, M.; Neidle, S.; Parkinson, G. N. Structural basis for Telomeric G-quadruplex Targeting by Naphthalene Diimide Ligands. *J. Am. Chem. Soc.* **2012**, *134*, 2723−2731.
(28) Prato, G.; Silvent, S.; Saka, S.; Lamberto, M.; Kosenkov, D. Thermodynamics of Binding of di- and tetrasubstituted Naphthalene Diimide Ligands to DNA G-quadruplex. *J. Phys. Chem. B* **2015**, *119*, 3335−3347.
(29) Milelli, A.; Tumiatti, V.; Micco, M.; Rosini, M.; Zuccari, G.; Raffaghello, L.; Bianchi, G.; Pistoia, V.; Fernando, D. J.; Pera, B.; Trigili, C.; Barasoain, I.; Musetti, C.; Toniolo, M.; Sissi, C.; Alcaro, S.; Moraca, F.; Zini, M.; Stefanelli, C.; Minarini, A. Structure-Activity Relationships of Novel Substituted Naphthalene Diimides as Anticancer Agents. *Eur. J. Med. Chem.* **2012**, *57*, 417−428.
(30) Hampel, S. M.; Sidibe, A.; Gunaratnam, M.; Riou, J. F.; Neidle, S. Tetrasubstituted naphthalene diimide ligands with selectivity for telomeric G-quadruplexes and cancer cells. *Bioorg. Med. Chem. Lett.* **2010**, *20*, 6459−6463.
(31) Doria, F.; Nadai, M.; Sattin, G.; Pasotti, L.; Richter, S. N.; Freccero, M. Water soluble extended naphthalene diimides as pH fluorescent sensors and G-quadruplex ligands. *Org. Biomol. Chem.* **2012**, *10*, 3830−3840.
(32) Di Antonio, M.; Doria, F.; Richter, S. N.; Bertipaglia, C.; Mella, M.; Sissi, C.; Palumbo, M.; Freccero, M. Quinone methides tethered to naphthalene diimides as selective G-quadruplex alkylating agents. *J. Am. Chem. Soc.* **2009**, *131*, 13132−13141.
(33) Ohnmacht, S. A.; et al. A G-quadruplex-binding compound showing anti-tumour activity in an in vivo model for pancreatic cancer. *Sci. Rep.* **2015**, *5*, No. 11385.
(34) Bhattacharya, S.; Chaudhuri, P.; Jain, A. K.; Paul, A. Symmetrical bisbenzimidazoles with benzenediyl spacer: the role of the shape of the ligand on the stabilization and structural alterations in telomeric G-quadruplex DNA and telomerase inhibition. *Bioconjugate Chem.* **2010**, *21*, 1148−1159.
(35) Maji, B.; Kumar, K.; Kaulage, M.; Muniyappa, K.; Bhattacharya, S. Design and synthesis of new benzimidazole-carbazole conjugates for the stabilization of human telomeric DNA, telomerase inhibition, and their selective action on cancer cells. *J. Med. Chem.* **2014**, *57*, 6973−6988.
(36) Dhamodharan, V.; Harikrishna, S.; Bhasikuttan, A. C.; Pradeepkumar, P. I. Topology specific stabilization of promoter over telomeric G-quadruplex DNAs by bisbenzimidazole carboxamide derivatives. *ACS Chem. Biol.* **2015**, *10*, 821−833.
(37) Nimesh, H.; Sur, S.; Sinha, D.; Yadav, P.; Anand, P.; Bajaj, P.; Virdi, J. S.; Tandon, V. Synthesis and biological evaluation of novel bisbenzimidazoles as *Escherichia coli* topoisomerase IA inhibitors and potential antibacterial agents. *J. Med. Chem.* **2014**, *57*, 5238−5257.
(38) Gunaratnam, M.; Swank, S.; Haider, S. M.; Galesa, K.; Reszka, A. P.; Beltran, M.; Cuenca, F.; Fletcher, J. A.; Neidle, S. Targeting human gastrointestinal stromal tumor cells with a quadruplex-binding small molecule. *J. Med. Chem.* **2009**, *52*, 3774−3783.
(39) Arora, A.; Balasubramanian, C.; Kumar, N.; Agrawal, S.; Ojha, R. P.; Maiti, S. Binding of berberine to human telomeric quadruplex - spectroscopic, calorimetric and molecular modeling studies. *FEBS J.* **2008**, *275*, 3971−3983.
(40) Arora, A.; Maiti, S. Differential biophysical behavior of human telomeric RNA and DNA quadruplex. *J. Phys. Chem. B* **2009**, *113*, 10515−10520.
(41) Dasso, M. *Current Protocols in Cell Biology*; John Wiley & Sons, Inc., 2005; Chapter 18.
(42) Perry, P. J.; et al. 1,4- and 2,6-disubstituted amidoanthracene-9,10-dione derivatives as inhibitors of human telomerase. *J. Med. Chem.* **1998**, *41*, 3253−3260.
(43) Kumar, N.; Basundra, R.; Maiti, S. Elevated polyamines induce c-MYC overexpression by perturbing quadruplex-WC duplex equilibrium. *Nucleic Acids Res.* **2009**, *37*, 3321−3331.
(44) Das, A.; Bhadra, K.; Kumar, G. S. Targeting RNA by small molecules: comparative structural and thermodynamic aspects of aristololactam-β-D-glucoside and daunomycin binding to tRNA(phe). *PLoS One* **2011**, *6*, No. e23186.
(45) Chauhan, A.; Paul, R.; Debnath, M.; Bessi, I.; Mandal, S.; Schwalbe, H.; Dash, J. Synthesis of Fluorescent Binaphthyl Amines That Bind c-MYC G-Quadruplex DNA and Repress c-MYC Expression. *J. Med. Chem.* **2016**, *59*, 7275−7281.
(46) Haudecoeur, R.; Stefan, L.; Denat, F.; Monchaud, D. A model of smart G-quadruplex ligand. *J. Am. Chem. Soc.* **2013**, *135*, 550−553.
(47) De Cian, A.; Guittat, L.; Kaiser, M.; Saccà, B.; Amrane, S.; Bourdoncle, A.; Mergny, J. L.; et al. Fluorescence-based melting assays for studying quadruplex ligands. *Methods* **2007**, *42*, 183−195.
(48) Arora, A.; Maiti, S. Effect of loop orientation on quadruplex-TMPyP4 interaction. *J. Phys. Chem. B* **2008**, *112*, 8151−8159.
(49) Wang, Y.; Patel, D. Solution structure of the human telomeric repeat d[AG3(T2AG3)3] G-tetraplex. *Structure* **1993**, *1*, 263−282.
(50) Parkinson, G. N.; Lee, M. P.; Neidle, S. Crystal structure of parallel quadruplexes from human telomeric DNA. *Nature* **2002**, *417*, 876−880.
(51) Huey, R.; Morris, G. M. *Using AutoDock 4 with AutoDocktools: A Tutorial*; The Scripps Research Institute, 2008; pp 54−56.
(52) Parkinson, G. N.; Cuenca, F.; Neidle, S. Topology conservation and loop flexibility in quadruplex-drug recognition: crystal structures of inter- and intramolecular telomeric DNA quadruplex-drug complexes. *J. Mol. Biol.* **2008**, *381*, 1145−1156.
(53) Micco, M.; Collie, G. W.; Dale, A. G.; Ohnmacht, S. A.; Pazitna, I.; Gunaratnam, M.; Reszka, A. P.; Neidle, S. Structure-based design and evaluation of naphthalene diimide G-quadruplex ligands as telomere targeting agents in pancreatic cancer cells. *J. Med. Chem.* **2013**, *56*, 2959−2974.
(54) Case, D. A.; Cheatham, T. E.; Darden, T.; Gohlke, H.; Luo, R.; Merz, K. M., Jr.; Onufriev, A.; Simmerling, C.; Wang, B.; Woods, R. J. The Amber Biomolecular Simulation Programs. *J. Comput. Chem.* **2005**, *26*, 1668−1688.
(55) Ryckaert, J. P.; Ciccotti, G.; Berendsen, H. J. C. Numerical integration of the Cartesian Equations of Motion of a System with Constraints: Molecular Dynamics of n-Alkanes. *J. Comput. Phys.* **1977**, *23*, 327−341.
(56) Humphrey, W.; Dalke, A.; Schulten, K. VMD: visual molecular dynamics. *J. Mol. Graphics* **1996**, *14*, 33−38.
(57) Pettersen, E. F.; et al. UCSF Chimera-a visualization system for exploratory research and analysis. *J. Comput. Chem.* **2004**, *25*, 1605−1612.
(58) *Maestro*, version 9.3, Schrodinger LLC: New York, NY, 2012.
(59) Fogolari, F.; Brigo, A.; Molinari, H. Protocol for MM/PBSA molecular dynamics simulations of proteins. *Biophys. J.* **2003**, *85*, 159−166.
(60) Miller, B. R., III; et al. MMPBSA.py: An Efficient Program for End-State Free Energy Calculations. *J. Chem. Theory Comput.* **2012**, *8*, 3314−3321.
(61) Kamran, M. Z.; Rajiv, P. G. Preclinical evaluation of the antimetastatic efficacy of Pentoxifylline on A375 human melanoma cell line. *Biomed. Pharmacother.* **2012**, *66*, 617−626.

DOI: 10.1021/acsomega.6b00523
ACS Omega 2017, 2, 966−980